Complex Optical Index of PbS Nanocrystal Thin Film and their Use for Short Wave Infrared Sensor Design

Bilal Chehaibou, Eva Izquierdo, Audrey Chu, Claire Abadie, Mariarosa Cavallo, Adrien Khalili, Tung Huu Dang, Charlie Greboval, Xu Xiangzhen, Sandrine Ithurria, et al.

Complex Optical Index of PbS Nanocrystal Thin Film and their Use for Short Wave Infrared Sensor Design

View Article Online
DOI: 10.1039/D1NR07770H

Bilal Chehaibou[1], Eva Izquierdo[2], Andrey Chu[2] Claire Abadie[3], Mariarosa Cavallo[2], Adrien Khalili[2], Tung Huu Dang[2], Charlie Gréboval[2], Xiang Zhen Xu[4], Sandrine Ithurria[4], Grégory Vincent[3], Bruno Gallas[2], Gabriel Mugny[5], Arthur Arnaud[6], Emmanuel Lhuillier[2*], Christophe Delerue[1*]

[1]Univ. Lille, CNRS, Centrale Lille, Univ. Polytechnique Hauts-de-France, Junia, UMR 8520 - IEMN, F-59000 Lille, France
[2]Sorbonne Université, CNRS - UMR 7588, Institut des NanoSciences de Paris, INSP, F-75005 Paris, France
[3]ONERA - The French Aerospace Lab, 6, chemin de la Vauve aux Granges, BP 80100, 91123 Palaiseau, France.
[4] Laboratoire de Physique et d'Etude des Matériaux, ESPCI-Paris, PSL Research University, Sorbonne Université Univ Paris 06, CNRS UMR 8213, 10 rue Vauquelin 75005 Paris, France.
[5]STMicroelectronics, 12 rue Jules Horowitz, 38019 Grenoble, France.
[6]STMicroelectronics, 850 rue J. Monnet, 38926 Crolles, France.

Abstract: As nanocrystals (NCs) gain maturity, they become central building blocks for optoelectronics in devices such as solar cells and, more recently, infrared focal plane arrays. Now that proof of concept of these devices has been established, their optimization requires a deeper understanding of their electronic and optical features to engineering their optoelectronic properties accurately. Though PbS NCs have been extensively investigated, the complex optical index of PbS NC thin films remains mostly unknown. Some previous works have unveiled the optical index for this type of material optimized for solar cells (excitonic peak at 940 nm), but longer wavelengths remain scarce and surface chemistry effects, which are known to be of central importance for the layer doping, are simply unexplored. Here, we conduct a systematic investigation of the complex optical index of PbS NC thin films using broadband spectrally resolved ellipsometry. The obtained results are then compared with simulations combining Tight-Binding (TB) modeling at the NC level and Bruggeman model to expand the results to the film scale. While TB calculation gives the NC optical indices, we extract keys NC film parameters as the NC volume fraction and ligand indices by fitting Bruggeman formula to ellipsometry measurement. We also bring evidence that this joint modeling method can be conducted without the need for ellipsometry data while preserving the main feature of the experimental result. Finally, the unveiled optical indices are used to model the absorption of short-wave infrared diode stack based on PbS NCs and are relevant for state-of-the-art devices. Our electromagnetic modeling shows that the absorption within the contact is now a major limitation of the current device operated at telecom wavelength.

Keywords: PbS, short wave infrared, light sensing, tight binding simulation, complex refractive index.

*To whom correspondence should be sent: christophe.delerue@iemn.fr and el@insp.upmc.fr

Introduction

Nanocrystals (NCs) initially developed for their bright tunable photoluminescence in the visible appear equally promising for infrared optoelectronics.[1] PbS is certainly the most mature colloidal material in this spectral range.[2] It combines a strongly tunable cut-off wavelength from 800 to 2000 nm with a low polydispersity level favorable to forming of high-quality films.

Integration of PbS NCs into a photodiode was initially motivated by the design of solar cells.[3] Compared to bulk material, PbS NCs enable the optimal optical gap for single-junction solar cells (≈1.3 eV) and benefit from the reduced threshold for multiexciton generation.[4–7]

At this absorption energy, the diode structure has been extensively optimized, and systematic investigation[8] of the relationship between surface chemistry and nature of the majority carrier has allowed a rational design of a *pn* junction.[9] The current best diode stack relies on ITO/ETL/PbS (*n*-type capped with halide)/PbS(*p*-type capped with thiol)/gold. Here, ITO stands for tin-doped indium oxide used as transparent conductive contact, while ETL means electron transport layer and is generally based on either ZnO[10] or TiO_2.[11] This diode stack achieves high internal quantum efficiency that suggests optimal charge separation and band alignment. This hypothesis was further supported by later uses of this structure for LED design.[12,13]

Beyond solar cells, PbS spectral range also matches other light-sensing applications in the short-wave infrared (SWIR), such as facial recognition for smartphones or industrial vision. In particular, in the SWIR, water presents a strong absorption band (at 1400 nm), enhancing the contrast with respect to the visible in which water is transparent.[13] Thus, it appears meaningful to expand the spectral range of PbS NCs based sensors beyond 1000 nm and explore wavelengths up to 1550 nm. Several reports in the literature already provide those types of diode stacks operated from 1200 to 1550 nm with impressive external quantum efficiency reaching 80 %.[10,14]

Further improvement requires a deep understanding of the current device performance to reveal the current bottlenecks and where future efforts must be focused. Here, we investigate the optical part of the device. So far and contrary to II-VI compounds,[15–17] the complex optical index of PbS NC films in the SWIR has been studied in a small number of experimental works[18–21] but an in-depth study of this quantity which is the main input of all electromagnetic simulations remains absent. In this paper, we used spectroscopic ellipsometry measurement to provide a systematic investigation of the effect of particle size and surface chemistry on the complex optical index NC thin film. We show an increase in the indices by shortening the ligand length and increasing the NC diameter. We coupled these results with simulations based on the Effective Medium Approximation (EMA) incorporating Tight-Binding (TB) electronic structure calculations to provide a better insight. The EMA models were mainly used for dilute systems[22–29] but have recently shown great promise to NC thin films.[18,30–32] However, to our knowledge, the coupling of electronic structure calculation with EMA models has not been reported. This joint modeling method reveals useful parameters of the NC film as the NC volume fraction and the index of the surrounding medium which integrates the ligand shell. Assuming that the latter can be used for different film compositions as the ligand is unchanged, we demonstrate that the NC film complex optical index could be fully computed using a hard-sphere model.

Furthermore, we inject the unveiled complex optical indices into electromagnetic simulations of relevant PbS NCs based diode stacks and map out their absorption properties.[20] We show that the calculated complex optical index as input correctly describes the NC absorption. Thus, it would permit to probe diverse composition photodiode performances. Moreover, we present evidence that absorption loss within the contact is a major limitation and propose new directions to tackle it.

Results and discussion

We start by growing a series of PbS NCs with an exciton peak from 1000 to 1550 nm, see **Figure 1**c. For this purpose, we used the procedure of Moreels *et al.*,[22,33] in which $PbCl_2$ is reacted with sulfur in oleylamine (OLA). The reaction temperature and its duration are used as the main knobs to tune the particle size. A warmer and longer reaction leads to larger particles. As suggested by Moreels *et al.*,[33] TOP is introduced during the synthesis of the smallest particles to slow the growth rate. Though the exact shape is a truncated cube, the particles present a quasi-sphere shape for all particle size as revealed by transmission electron microscopy (TEM), see **Figure 1**a-b and S1. We thus assume a random close packing in all cases. The NC diameter increases from 4.5 nm for a particle with an excitonic peak at 1000 nm to 7.5 nm for a particle presenting an exciton at telecom wavelength (1550 nm), see **Table 1** and S1. Subsequently, in the rest of the article, each population of PbS will be referred to its peak wavelength (*i.e.,* PbS 1200 will refer to the population with an exciton feature at 1200 nm).

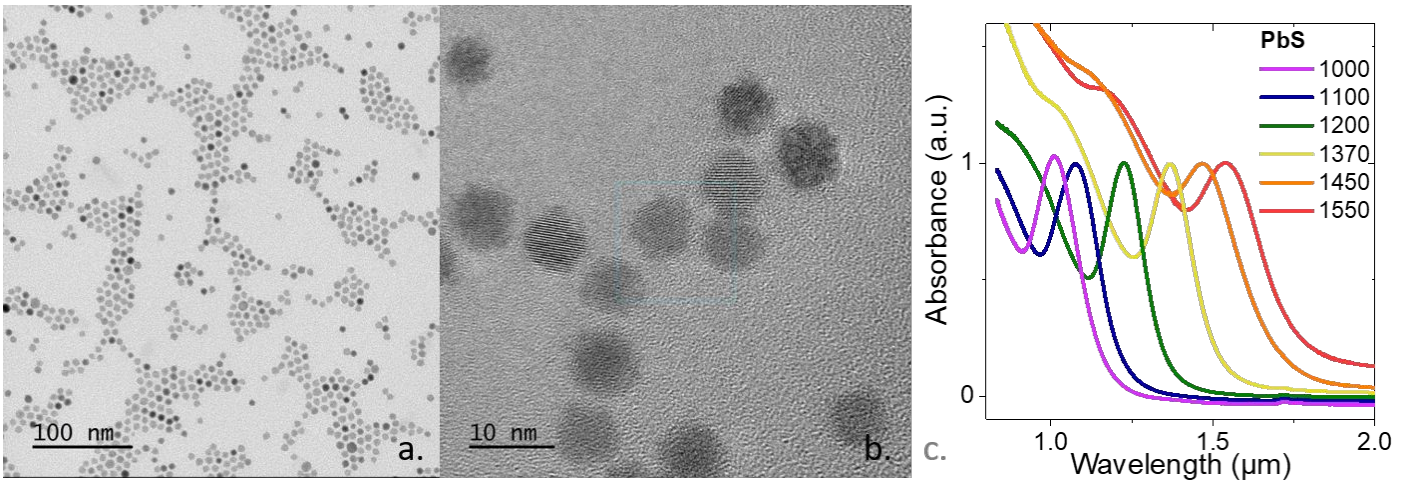

***Figure 1 PbS nanocrystals**. TEM (a.) and high resolution TEM (b.) of PbS 1550 sample. c. Absorption spectra for a series of PbS NCs with excitonic peak from 1000 to 1550 nm.*

***Table 1 Spectroscopic and structural parameters of the PbS NCs.** The average refractive index is calculated over the wavelength range 750-2000 nm.*

	PbS 1000	PbS 1100	PbS 1200	PbS 1370	PbS 1450	PbS 1550
Particle diameter (nm)	4.5±1.5	4.6±1.1	5.2±0.8	6.1±1.4	6.6±1.3	6.7±1.1
Exciton peak (nm/cm^{-1}/meV)	1012 nm 9880 cm^{-1} 1225 meV	1078 nm 9270 cm^{-1} 1150 meV	1223 nm 8172 cm^{-1} 1013 meV	1370 nm 7300 cm^{-1} 905 meV	1465 nm 6825 cm^{-1} 846 meV	1533 nm 6520 cm^{-1} 808 meV
Average refractive index (OA capping)	1.84±0.1	1.81±0.1	1.95±0.1	2.04±0.1	2.17±0.1	2.04±0.1

We deposit the PbS material to form a thin film onto a transparent glass substrate. In addition, for three particle sizes, we also perform ligand exchange to probe the effect of the surface chemistry on the optical properties. We choose PbS 1200, PbS 1370, and PbS 1550. PbS 1200 and 1370 have been chosen because they are close to the water absorption edge and spectrally on each side of the absorption. PbS 1550 has been chosen to match the telecom wavelength and the associated broad range of source, which enable active imaging for example in autonomous vehicle. Regarding

the surface chemistry, we have focused on ethanedithiol (EDT) and iodide ion (I^-), respectively, for their ability to form *p*- and *n*-type layers in the case of small-sized PbS NCs.

These films have been characterized by spectrally resolved ellipsometry in the 450 to 2000 nm range. Ellipsometry measured the change of the polarization of light upon its reflection on the NC film. The two angles (ψ;Δ) associated with this change are measured. To retrieve these angles, the dielectric constant is then fitted by a sum of oscillators, see Figure S2. As a consequence, from this dielectric constant, one can estimate the values of ψ and Δ. Using a least-square fit procedure, the parameters of the fit are optimized to minimize the difference between the measured and estimated (ψ;Δ) values. To reduce possible errors, the measurements are conducted using three angles for incidence: 50°, 60°, and 70° (see Figure S3). In addition, we do not introduce oscillators at wavelengths beyond the exciton in order for *k* to converge to zero at low energy. We provide in **Figure 2a-c** the determined refractive index (*n*) and extinction coefficient (*k*) for the sample of PbS 1200 capped with the three ligands. Data for other wavelengths are available in Figure S4 (for size dependence), and S5 (for three surface chemistries), and all raw data spectra are provided as supporting files.

View Article Online
DOI: 10.1039/D1NR07770H

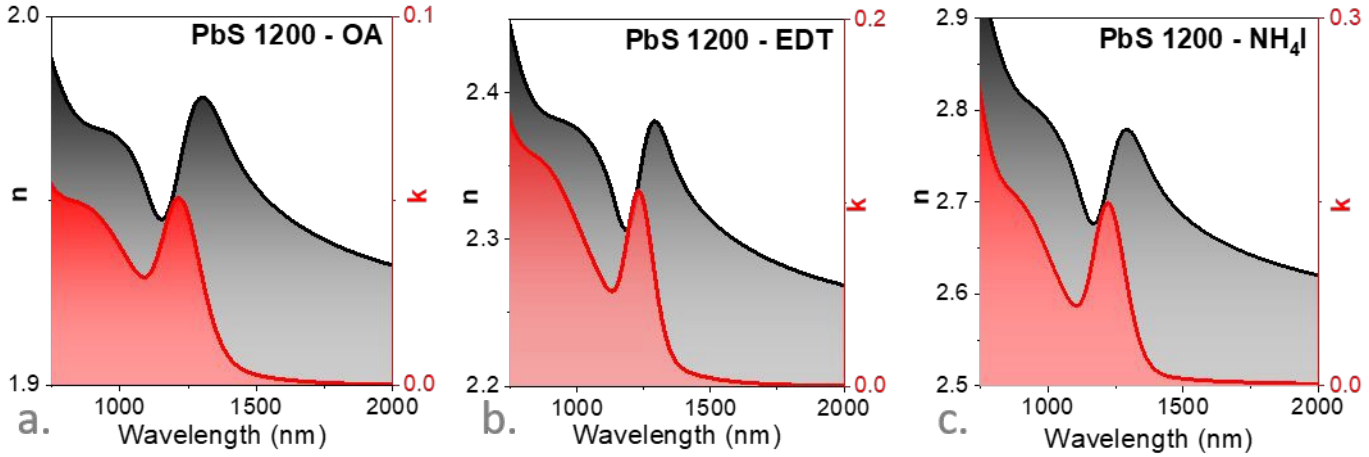

***Figure 2 Refractive index and extinction coefficient spectra for PbS 1200** capped with oleic acid (a.), EDT (b.) and NH_4I (c.). Data for PbS 1370 and 1550 are provided in Figure S5.*

Figure 3a clearly shows an increase of the average refractive index of the NC film from 1.8 to 2.15 as the particle size is increased, which can be connected to the higher volume fraction (f_{NC}) of the NCs (**Figure 3**c, see below). Another strategy to tune the volume fraction is to change the particle surface chemistry from oleic acid (OA) ligands to I^-. OA ligands are typically ≈1.5 nm long, while EDT are ≈0.5 nm and I^- around ≈0.3 nm.[34] As a result, the refractive index increases from 1.95 for OA to 2.35 for EDT and finally to 2.7 for I^- (**Figure 2** and **Figure 3**b). The same reason explains a drastic rise of the extinction coefficient, which almost triples as OA ligands are replaced by iodine (**Figure 3**d). A similar trend is observed for all particle sizes (see Figure S5).

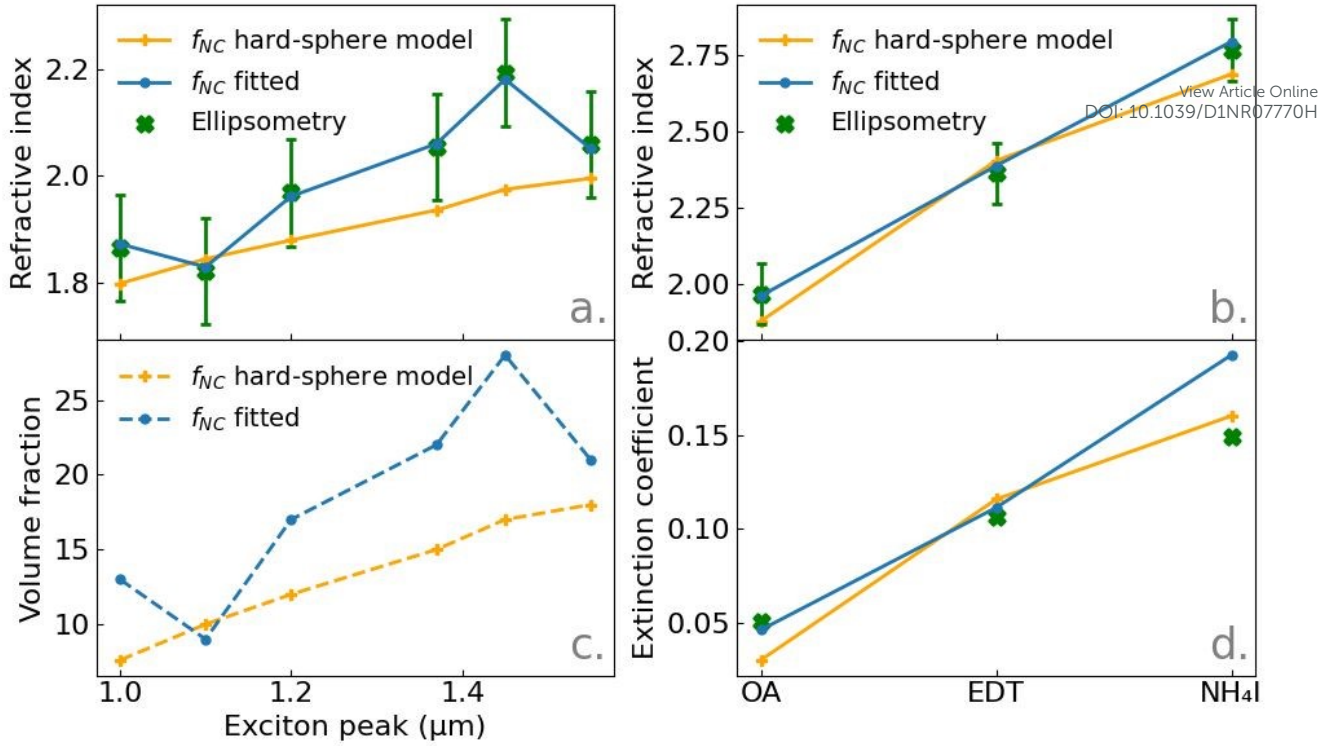

Figure 3 Comparison between data extracted from ellipsometry measurements *(green crosses)* ***and Bruggeman simulations,*** *in which the NC volume fraction was either fitted (blue) or computed with a hard-sphere model (orange), as a function of the exciton peak wavelength for OA capping (a,c) or as a function of the capping for PbS 1200 nm (b,d). a-b. Refractive index averaged over the 750 to 2000 nm range. c. NC volume fraction. d. Extinction coefficient.*

The importance of surface chemistry on the complex refractive index is visible in **Figure 4**, in which we present the same data as **Figure 2** for PbS 1200 (Figure S5 for other particle sizes) but using common vertical axes allowing direct comparison. In order to have a deeper insight into these evolutions, we used an Effective Medium Approximation (EMA) coupled with TB calculations to simulate the complex refractive index and compare it with ellipsometry measurements. Two EMAs, Maxwell Garnett, and Bruggeman[35,36] are compared in SI, while the latter is presented in the main text. Indeed, due to its symmetry, the Bruggeman formula is better suited when the NC volume fraction f_{NC} approaches the host one. The Bruggeman formula is given by:

$$f_{NC}\frac{\varepsilon_{NC}-\varepsilon}{\varepsilon_{NC}+2\varepsilon}+(1-f_{NC})\frac{\varepsilon_h-\varepsilon}{\varepsilon_h+2\varepsilon}=0 \qquad (1)$$

ε_{NC}, ε_h, and ε are the complex dielectric functions for the NC, the host, and the medium, respectively $(n+ik=\sqrt{\varepsilon})$. ε_{NC} is computed from TB calculations (Method Section), while ε_h and f_{NC} are used as fitting parameters to reproduce ellipsometry measurements. Note that ε_{NC}, the dielectric constant of the pristine NC in **Figure 5**, presents much larger values of the refractive index (n > 3.4) than the one observed from the film.

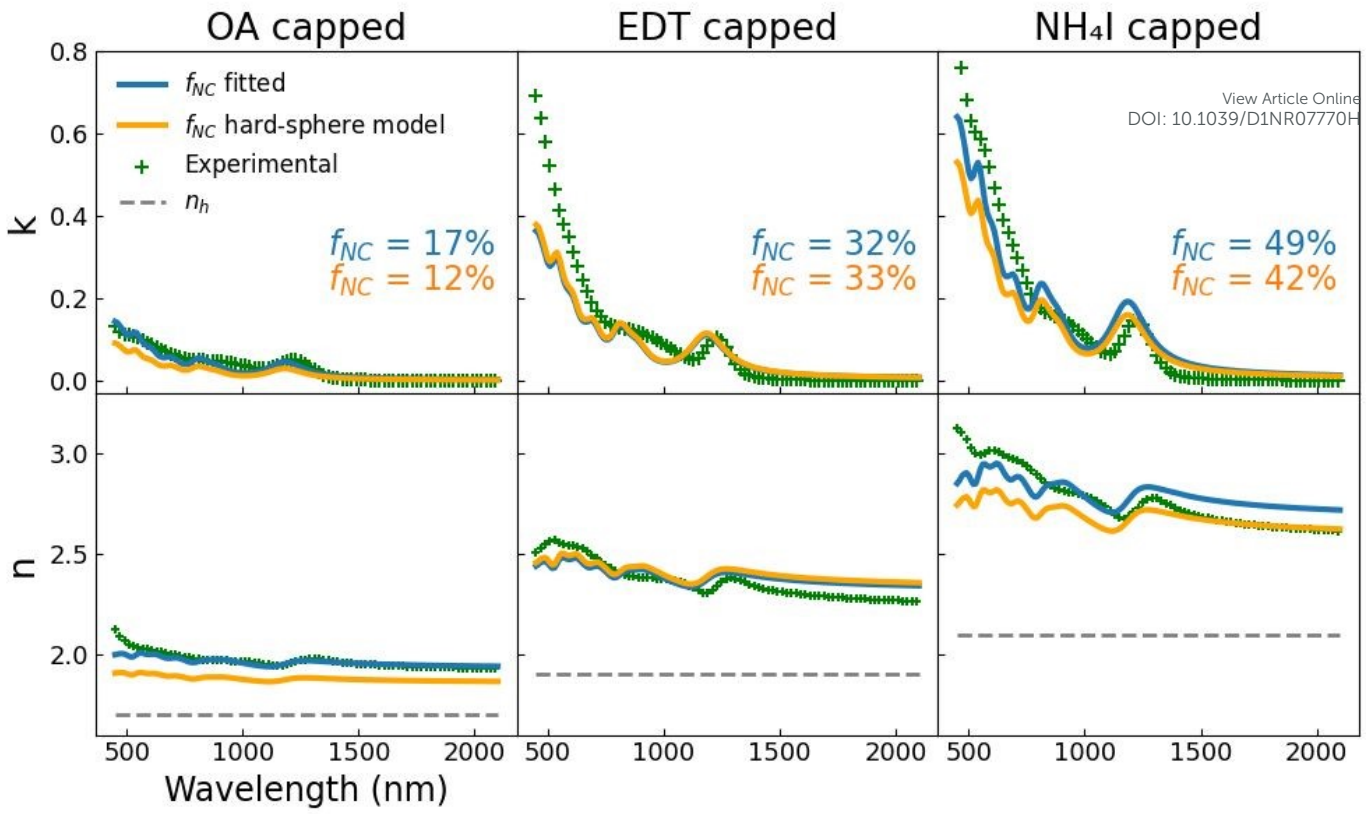

Figure 4 Refractive index (n) and extinction coefficient (k) for PbS 1200 *capped with OA, EDT, and NH_4I. The theoretical indices (full lines) obtained with Bruggeman approximation, in which the NC volume fraction (f_{NC}) is either fitted (blue) or computed by the hard-sphere model (orange), are compared with the ellipsometry measurements (green crosses). The grey dashed line denotes the host refractive index: 1.7, 1.9 and 2.1 for OA, EDT, and NH_4I, respectively.*

The method of extraction of ε_{NC}, ε_h and f_{NC} to solve the film permittivity ε is detailed in the Method Section. We also considered an alternative approach by taking the NC volume fraction (f_{NC}) given by the hard-sphere model (Equation 3, Method Section). **Figure 4** compares the complex refractive index for the PbS 1200 film measured by ellipsometry and computed with the Bruggeman approximation. The data for PbS 1370 and 1550 are given in SI. The refractive index of ligands (n_h) obtained for OA, EDT, and NH_4I are 1.7, 1.9, and 2.1, respectively. As n_h mainly depends on the host, we assume these values transposable to any NC thin film, as the ligands keep unchanged, allowing to remove one free parameter. The fitted (hard-sphere model) volume fractions f_{NC} are 17(12), 32(33), and 49(42) percent for OA, EDT, and NH_4I, respectively. In accordance with the experimental results, the volume fraction of NCs increases with the shortening of the length of the ligand. This leads to an increase of the complex refractive index due to the inorganic matter quantity growing in the film (**Figure 3b**,**d**; **Figure 4**).

View Article Online
DOI: 10.1039/D1NR07770H

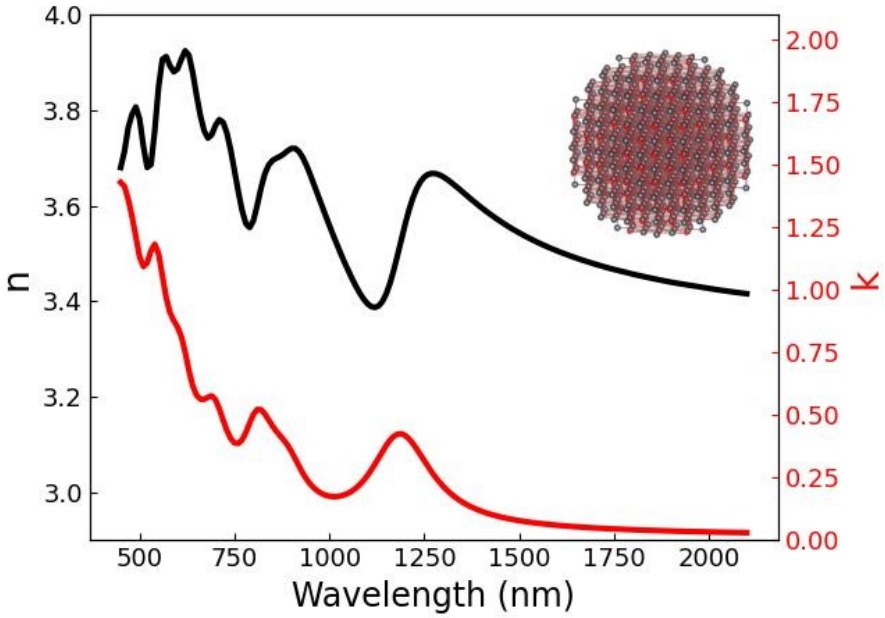

Figure 5 Optical indices calculated in TB for a single PbS NC with the lowest exciton at 1200 nm. *The refractive index (black line) and extinction coefficient (red line) are computed using the TB electronic structure of a 2-nm-diameter NC (upper right insert).*

As found by Dement et al.,[31] the volume fractions obtained with the hard-sphere model match those fitted from experiments using the Bruggeman model (**Figure 3c** and **Figure 4**). However, we observe a slight underestimation for the hard-sphere model, also visible when we vary the NC size. As suggested by Diroll et al.,[16] a picture of hard cores with rigid organic shells overestimates the denominator term of Equation 3 (Method Section), leading to an underestimation of f_{NC}. Despite this, both theoretical calculations (fitted and hard-sphere model) give spectral features, excitonic and higher-order peaks, in reasonable agreement with experiments. Moreover, the quantitative evolution of the extinction coefficient and the average refractive index with surface chemistry and with size (**Figure 3** and **Figure 4**) follows the ellipsometry data. Here, we bring evidence that EMA models coupled with electronic structure calculations allow to unveil films parameters as the NC volume fraction. Adding another theory layer with the analytical hard-sphere model and using known ligand optical indices, this parameter-free model (see Equation 1) grants direct film optical index calculation.

Thereafter, we aim to use the complex optical indices to reveal the absorption properties of a diode stack used for SWIR sensing. We consider the most typical stack[9,14] based on ITO/TiO_2/PbS(n-type capped with halide)/PbS(p-type capped with thiol)/gold. Geometrical parameters are provided in the SI. To vary the optical gap of the diode, we tune the cut-off wavelength of the PbS *n*-type layer, while keeping for all diodes the same type of NCs, and in particular the *p*- type layer (PbS 1200 with EDT capping). Indeed, PbS capped with thiol experiences a crossover from *p* doped to *n* doped with size.[37] As for ellipsometry data, Figure **6** focuses on PbS 1200, and similar data are provided in the SI for diodes at 1370 nm (Figure S13) and 1550 nm (Figure S14).

In all that follows, the spectral dependence of both n and k has been included in our simulation. Nevertheless, we notice that the spectral dependence of the refractive index is weak, $\Delta n(\lambda)/\langle n(\lambda)\rangle \approx 5-10\%$ where $\langle n(\lambda)\rangle$ is the spectrally averaged value of n and $\Delta n(\lambda) = n(\lambda) - \langle n(\lambda)\rangle$. In **Figure 6**b and S11, we have simulated the absorption spectra for the three diodes, either accounting for

View Article Online
DOI: 10.1039/D1NR07770H

entire spectral dependence or using the average spectral value of n instead. It appears that the spectra remain primarily unchanged. In particular, the features close to the optical gap are well reproduced. This observation may ease future measurements since spectrally resolved measurement of the refractive index may not be required unless high accuracy simulations are targeted. Additionally, we have simulated the absorption spectrum of the full diode stack while using the $(n;k)$ values obtained directly from the TB simulation, assuming for simplicity the hard-sphere model (**Figure 6**b). In this case, even though the agreement is not as good, it remains very reasonable, meaning that TB calculations can be used for scaling rule of design.

In **Figure 6**a, we have plotted the absorption (taken equal to 1-R, R the reflection since transmission is null due to gold mirror) spectra within the NC film (*i.e.,* excluding the loss in the contact) as a function of the thickness of the I^- capped PbS layer. We observe a modulated horizontal line at ≈1200 nm corresponding to the exciton, while a series of tilted lines result from resonances. As these resonances reach the exciton energy, a strong modulation of the absorption amplitude is observed for the energy corresponding to the exciton. The nature of the resonances is better revealed by the dispersion map, see **Figure 6**d. There is almost no dispersion (*i.e.,* no k_x dependence) which is typical of a Fabry-Pérot resonance. Such resonances may have been anticipated given the simplicity of the structure (no grating or any subwavelength resonator).

The presence of this resonance makes the absorption at the exciton non-monotonic with thickness. As a result, a 330 nm thick layer is more absorbing than a 400 nm layer, while it also enables a better charge collection since the thickness better matches the short carrier diffusion length induced by hopping. With 75 % of absorption, a 330 nm thick layer typically absorbs twice as much as the same layer not included in the diode structure ($1-\exp\left(\frac{-4\pi kt}{\lambda}\right)$ with t the device thickness and λ the wavelength). The absorption map (**Figure 6**c) better explains why we observe a non-monotonic increase of the absorption with thickness. In this stack, the absorption appears as a standing wave with core and node, and the period D of this wave is given by $\lambda = 2nD$. For a resonance at ≈1200 nm and $n = 2.7$ as measured for I^- capped PbS, this leads to $D = 230$ nm. Thus, if the thickness is increased but only includes an area corresponding to a node of the absorption, the increase of absorption is very weak. We observe a significant increase of absorption only when the thickness is increased by $\approx D$. However, building thicker devices may become challenging and may not lead to an efficient charge collection. Finally, it is worth pointing that, at 1200 nm, the absorption is spatially located within the NCs, and losses in ITO and metal remain weak.

An interesting question to ask at this point: would there be any optical benefit of tuning the relative thickness of the *n* and *p* type layer? Figure S12 proposes a map of the absorption in the NCs as a function of *n* and *p* type layer thicknesses. The resonance lines of the exciton exactly follow the iso-thickness curve, meaning that increasing the *p*-type layer brings no benefit and that only the total thickness plays an actual role. Thus, the relative choice of thickness between the two layers will be rather dictated by electrostatic (formation of the *pn* junction) and technological (building a thick *p* layer from solid-state ligand exchange is likely more difficult) considerations.

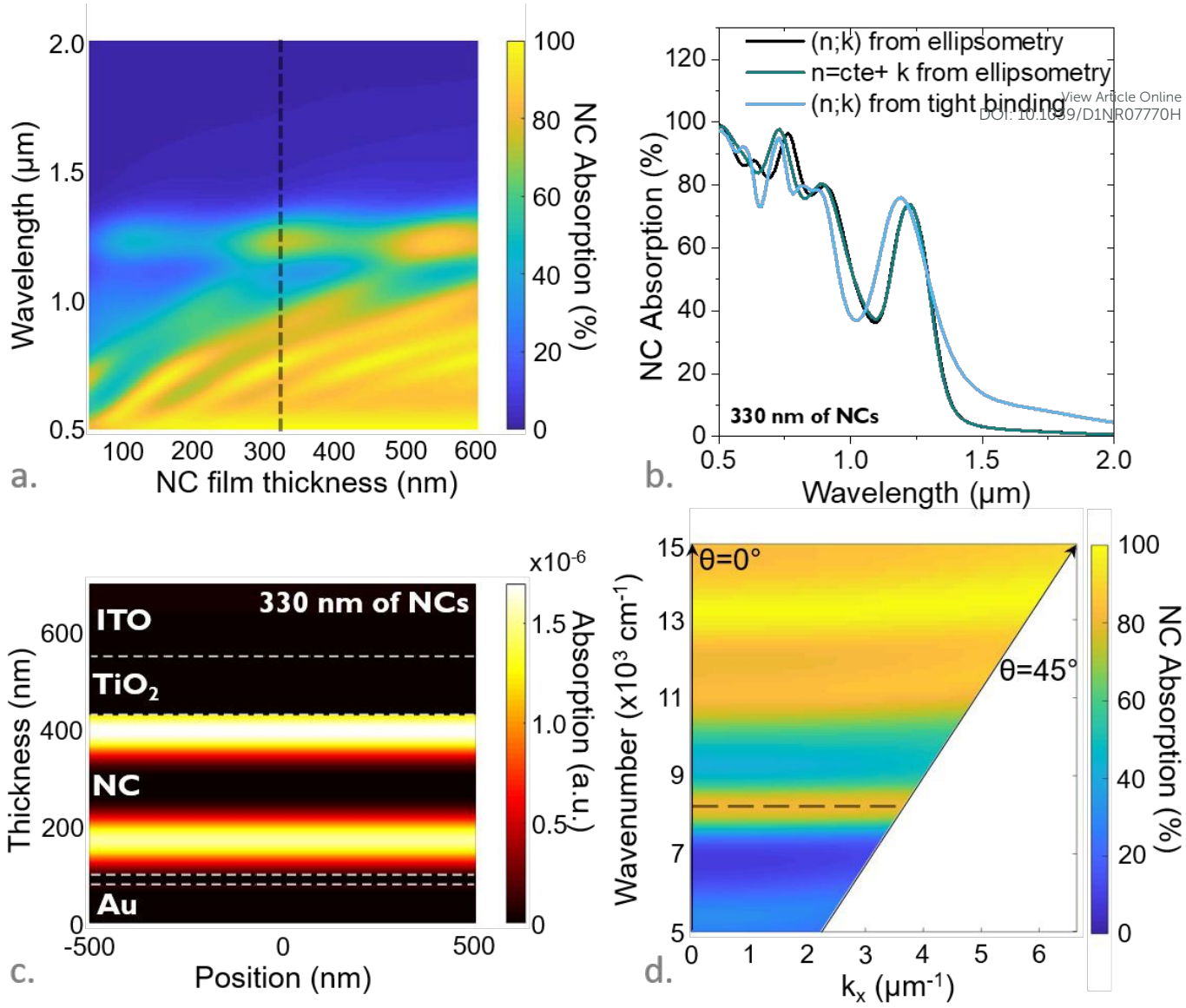

Figure 6 Simulation of diode absorption based on refractive index and extinction coefficient revealed by ellipsometry and modelling. *a. Absorption within the NCs for a diode made of PbS 1200 as a function of the wavelength and thickness of the n-type NH_4I capped PbS layer. b. Absorption spectra within the NCs for a diode made of PbS 1200 for a 330 nm thickness of the n-type NH_4I capped PbS layer. c. Absorption spatial map for a diode made of PbS 1200. d. Dispersion relation (wavenumber as a function of k_x wavevector) for a diode made of PbS 1200.*

As the cut off wavelength of the diode is increased (*i.e.,* the one from the n-type layer with I^- capping, see Figure S13 and S14), some results remain unchanged: (*i*) we keep observing a series of non-dispersive resonances which can be attributed to a Fabry-Pérot cavity within the diode stack, and (*ii*) the absorption map is still the result of a standing wave. However, there are also some apparent differences. Thin devices are only poorly absorbing, and only devices thicker than 500 nm can achieve absorption above 50 %. This makes the recent development of µm thick films of utmost interest.[38] Secondly, losses in the contacts become non-negligible, both in gold and ITO. For the sake of illustration, we have estimated the loss in the ITO layer for the diode based on PbS 1550, see Figure S15. In this case, 15 % of the total absorption occurs in the ITO. This makes the recent report of 80 % of external quantum efficiency on a similar diode operating at 1.55 µm even more impressive.[14] Because absorption is already large, there will be only a limited benefit to introduce light resonators[39] to increase the light absorption (+25 % at best). Resonators might still be interesting from a transport point of view since charge collection is also more efficient in thin

devices.[15] Reducing the loss in contacts is probably the next important challenge. Gold remains a moderate problem at this wavelength, and its use as both hole extractor and mirror makes it difficult to reduce the thickness. Thus, a first obvious optimization strategy will be to reduce the ITO thickness, but this will come at the price of higher contact resistance. Optimizing conditions of ITO growth has also been proposed as a possible strategy.[40] We probably reach a point where an alternative material for contact will have to be explored. Graphene[41,42] or silver nanowires array[43] are certainly possible strategies combining high infrared transparency, high conductivity, and large-scale availability.

View Article Online
DOI: 10.1039/D1NR07776H

Conclusion

We have conducted a systematic investigation of the complex optical index of PbS NC film as a function of their size and surface chemistry, which is of utmost interest for the later optical design of devices based on these materials. The results are compared with simulations where the Tight-Binding method is used to determine the effective parameters at the particle level and where the Bruggeman model is also used to expand the result up to the macroscopic scale. This joint approach is useful to extract essential parameters of NC films, such as the NC volume fraction or the refractive index of the host. Moreover, we demonstrate that using a hard-sphere model (*i.e.,* without free parameters) and a fixed n_h (transferable to any size of NCs), optical indices with reasonable match with experimental data can be obtained. These indices can then be used as inputs for electromagnetic simulations to predict photonic device performance and propose new directions for experimental works.

Method section

Chemicals. trioctylphosphine (TOP, Alfa Aesar, 90%), oleylamine (Alfa Aesar, 80-90%), lead chloride ($PbCl_2$, Alfa Aesar, 99%), sulfur powder (S, Alfa Aesar, 99.5%), oleic acid (OA, Alfa Aesar, 90%), 1,2 ethanedithiol (EDT, Fluka, 98.0%), ethanol absolute anhydrous (VWR), methanol (VWR, 99.8%), acetone (VWR), n-hexane (VWR), n-octane (SDS, 99%), toluene (VWR, 99.3%), N,N-dimethylformamide (DMF, VWR), ammonium iodine (NH_4I, Alfa Aesar, ≥ 99%), acetonitrile (VWR, ACS), butylamine (Alfa Aesar, 99%). All chemicals are used as received, except oleylamine which is centrifuged before use.

PbS NC Synthesis. In a three-neck flask, 300 mg of $PbCl_2$ and 7.5 mL of OLA are degassed, first at room temperature and then at 110 °C for 30 min. For the smallest particles (ie with en exciton peak below or equal to 1200 nm), 100 µL of TOP is also introduced. Meanwhile 30 mg of S powder are mixed with 7.5 mL of OLA until full dissolution and a clear orange solution is obtained. Then under N_2 at a temperature between 80 and 150°C, this solution of S is quickly added to the flask. After 0.5 to 15 minutes, the reaction is quickly quenched by addition of 1 mL of oleic acid and 9 mL of hexane. The NCs are precipitated with ethanol and redispersed in toluene. This washing step is repeated one more time. The solution is then centrifuged to remove the unstable phase. The supernatant is precipitated with methanol and redispersed in toluene. The exact procedures for each size of particle are given in the supporting information.

Film deposition for ellipsometry measurements: After synthesis the NCs solution are filtered with a PTFE filter. A glass slide is cut (12x15 mm) and washed using an acetone bath in ultrasound for 5 min. The substrates are then rinsed with acetone and isopropanol and dried using a N_2 gun. The pristine samples are deposited on a glass substrate using spin coating (1500 rpm, 500 $rpm.s^{-1}$, 45 s). For the EDT ligand exchange the NC solution is diluted at 30 $mg.mL^{-1}$ in toluene. A layer is then deposited onto the substrate using spin coating (2000 rpm, 1000 $rpm.s^{-1}$, 45 s). The sample is then dipped into an EDT exchange solution (0.1%vol EDT in ACN) for 1 min and rinsed in pure ACN for 30s. This process is repeated one more time. For NH_4I ligand exchange, an ink is made. 1 mL of a saturated solution of NH_4I in DMF is added to 1 mL of the NC solution (in toluene). Hexane is added to help the phase dissociation. The apolar phase is discarded. 3 cleanings with hexane are conducted. NCs are precipitated using acetone. After centrifugation the liquid phase is discarded and the NCs are dispersed in a mix of 140 µL of DMF, 60 µL of ACN and 5 µL of butylamine. The ink is then spin coated onto the substrate (2000 rpm, 200 $rpm.s^{-1}$, 120 s). This ink is used for the PbS with an excitonic peak at 1200 nm and 1300 nm.
For the NCs with a peak at 1.5 µm, a solid-state ligand exchange is conducted. The NC solution is diluted at 30 $mg.mL^{-1}$ in toluene. A layer is then deposited onto the substrate using spin coating (2000 rpm, 1000 $rpm.s^{-1}$, 45 s). The sample is then dipped into an NH_4I exchange solution (60 mg of NH_4I in EtOH) for 1 min and rinsed in pure EtOH for 30s. This process is repeated one more time.

Infrared spectroscopy: The solution of NC is drop-casted on the diamond cell of an ATR of a Fourier Transform Infrared spectrometer (FTIR, Thermo Fischer iS50). The source is a halogen lamp, the beam splitters are made of a CaF_2 and the detector is a DTGS sensor. In all cases, the background uses the same optical configuration but without the sample onto the substrate. Spectra are typically acquired with a 4 cm^{-1} resolution and typically averaged 32 times.

Transmission electron microscopy: A drop of diluted NC solution was drop-casted onto a copper grid covered with an amorphous carbon film. The grid was degassed overnight under secondary vacuum. Imaging was conducted using a JEOL 2010 transmission electron microscope operated at 200 kV.

View Article Online
DOI: 10.1039/D1NR07770H

Optical ellipsometry: The spectroscopic ellipsometry measures the changes in the polarization state between the incident and the reflected light and is characterized by the angles ψ and Δ.

$$\rho = \frac{r_p}{r_s} = \left|\frac{r_p}{r_s}\right| e^{i(\delta_p - \delta_s)} = \tan\psi e^{i\Delta}$$

where r_p and r_s are the reflection coefficients of p and s polarized light respectively and where δ_p.and δ_p are the phase shifts in reflection in p and s polarizations, respectively. The measurements are performed on a V-VASE ellipsometer (J.A. Woollam) in the 450-2100 nm range with steps of 10 nm and with angles of incidence of 50°, 60° and 70°.

Tight-binding simulation: The Hamiltonian matrix, including the spin-orbit coupling, is constructed in an $sp^3d^5s^*$ basis. The TB parameters are listed Table S1. The resulting TB bulk band structure is in good agreement with ab initio calculations (Figure S6). With appropriate boundary conditions, the TB parameters are the same, from bulk to NCs. We used excitonic peak position to calibrate NC diameters and compare them to TEM measurements, Figure S7.

Nanocrystal complex dielectric function: The NC complex dielectric function is given by[44]:

$$\varepsilon_{NC} = 1 - \sum_{i,j} \frac{e^2 |\langle u_{c,i} | \boldsymbol{r}.\boldsymbol{e} | u_{v,j} \rangle|^2}{\varepsilon_0 \Omega} \left(\frac{1}{\hbar\omega - E_{c,i} - E_{v;j} + i\sigma} - \frac{1}{\hbar\omega + E_{c,i} - E_{v;j} + i\sigma} \right) [f_{v,j} - f_{c,i}] \qquad (2)$$

with $u_{c,i}$ and $u_{v,j}$the conduction and valence wave functions of energy $E_{c,i}$and $E_{v,j}$with the equilibrium population given by $f_{c,i}$ and $f_{v,j}$ given a Fermi-Dirac distribution. σ is a parameter accounting for the experimental broadening due to electron-phonon interactions and size polydispersity. It is obtained by fitting a Lorentzian to the excitonic peak of experimental data (PbS 1200 OA) and transferred without any change to the other NC films (see Figure S8). Ω is the volume of the NC, $\boldsymbol{e}$ is the polarization vector of the light and, $\boldsymbol{r}$ is the electron position.

Bruggeman model and parameters extraction: To solve ε from equation 1, the three following parameters need to be extracted: f_{NC}, ε_h , and ε_{NC} . The latter is determined via TB calculation using the equation 2. We consider that the imaginary part of ε_h equals zero because the host is assumed to be non-absorbing at the wavelength of interest. The real part ($\varepsilon_h = n_h^2$) is supposed to be constant over the spectral range as its frequency dependence is weak. Moreover, n_h is a NC independent parameter; in other words, it only depends on the host, including ligands, air, and any residual organics under a solid-state form. Thus, for each passivation type, we estimated it as the overall best value to fit the Bruggeman optical indexes to PbS 1200, 1370, and 1550 ellipsometry measurements. Once we determined ε_{NC} and n_h, we fitted f_{NC} by a least-squares minimization procedure on experimental data.

The f_{NC} has also been calculated by the hard-sphere model:

$$f_{NC} = PF \frac{r_{NC}^3}{r_{NC+ligand}^3} \qquad (3)$$

where a random-close-packed distribution assumes 64% packing fraction (PF). It has shown reasonable packing estimates for glassy films of CdSe NCs.[45] The length of the ligands in the films is taken close to the literature, including the interparticle spacing measured by Weidman *et al.*[34]: 1.5, 0.5, and 0.3 nm for OA, EDT, and NH_4I, and the NCs radii r_{NC} are those calibrated by TB.

Electromagnetic simulation: Calculations are achieved with Matlab library based on RCWA.[46] The Maxwell equations are solved in each layer and interface conditions are applied to find the final solution of the whole structure. We consider incoming plane waves under normal incidence, either with transverse magnetic (TM) or transverse electric (TE) polarizations, *i.e.* with a magnetic field or electric field parallel to the slits of the gratings, respectively.

ASSOCIATED CONTENT

Supplementary materials include (*i*) material synthesis and characterization, (*ii*) details about the procedure to perform ellipsometry measurements and a full ellipsometry data set for all wavelengths and surface chemistries, (*iii*) tight binding simulations and (*iv*) electromagnetic simulation procedure and additional results.

AUTHOR CONTRIBUTIONS

B. Chehaibou, G. Mugny, A. Arnaud, C. Delerue performed the modelling part.
M. Cavallo, A. Khalili, T. H. Dang, C. Gréboval, grow the particles under supervision of E. Lhuillier and S. Ithurria.
E. Izquierdo, conducted ellipsometry measurements and model the results under supervision of B. Gallas.
X. Z. Xu performed TEM imaging.
A. Chu and C. Abadie conducted the electromagnetic simulations under supervision of G. Vincent.

COMPETING INTEREST

The authors declare no competing financial interest.

ACKNOWLEDEGMENTS

Bilal Chehaibou and Christophe Delerue thank Jing Li and Benoit Sklenard for providing the band structure of bulk PbS. The project is supported by ERC starting grant blackQD (grant n° 756225). We acknowledge the use of clean-room facilities from the “Centrale de Proximité Paris-Centre”. This work has been supported by the Region Ile-de-France in the framework of DIM Nano-K (grant dopQD). This work was supported by French state funds managed by the ANR within the Investissements d'Avenir programme under reference ANR-11-IDEX-0004-02, and more specifically within the framework of the Cluster of Excellence MATISSE and also by the grant IPER-Nano2 (ANR-18CE30-0023-01), Copin (ANR-19-CE24-0022), Frontal (ANR-19-CE09-0017), Graskop (ANR-19-CE09-0026) and NITQuantum (ANR-20-ASTR-0008-01), Bright and MixDferro (ANR-21-CE09-0029.).

REFERENCES

(1) Lu, H.; Carroll, G. M.; Neale, N. R.; Beard, M. C. Infrared Quantum Dots: Progress, Challenges, and Opportunities. *ACS Nano* **2019**, *13*, 939–953.

(2) Hines, M. A.; Scholes, G. D. Colloidal PbS Nanocrystals with Size-Tunable Near-Infrared Emission: Observation of Post-Synthesis Self-Narrowing of the Particle Size Distribution. *Adv. Mater.* **2003**, *15*, 1844–1849.

(3) Nozik, A. J. Quantum dot solar cells. *Phys. E Low-dimensional Syst. Nanostructures* **2002**, *14*, 115–120.

(4) Klimov, V. I. Spectral and Dynamical Properties of Multiexcitons in Semiconductor Nanocrystals. *Annu. Rev. Phys. Chem.* **2007**, *58*, 635–673.

(5) Schaller, R. D.; Klimov, V. I. High efficiency carrier multiplication in PbSe nanocrystals: implications for solar energy conversion. *Phys. Rev. Lett.* **2004**, *92*, 186601.

(6) Semonin, O. E.; Luther, J. M.; Choi, S.; Chen, H.-Y.; Gao, J.; Nozik, A. J.; Beard, M. C. Peak external photocurrent quantum efficiency exceeding 100% via MEG in a quantum dot solar cell. *Science* **2011**, *334*, 1530–1533.

(7) Pijpers, J. J. H.; Ulbricht, R.; Tielrooij, K. J.; Osherov, A.; Golan, Y.; Delerue, C.; Allan, G.; Bonn, M. Assessment of carrier-multiplication efficiency in bulk PbSe and PbS. *Nat. Phys.* **2009**, *5*, 811–814.

(8) Brown, P. R.; Kim, D.; Lunt, R. R.; Zhao, N.; Bawendi, M. G.; Grossman, J. C.; Bulović, V. Energy level modification in lead sulfide quantum dot thin films through ligand exchange. *ACS Nano* **2014**, *8*, 5863–5872.

(9) Chuang, C.-H. M.; Brown, P. R.; Bulović, V.; Bawendi, M. G. Improved performance and stability in quantum dot solar cells through band alignment engineering. *Nat. Mater.* **2014**, *13*, 796–801.

(10) Bi, Y.; Pradhan, S.; Gupta, S.; Akgul, M. Z.; Stavrinadis, A.; Konstantatos, G. Infrared Solution-Processed Quantum Dot Solar Cells Reaching External Quantum Efficiency of 80% at 1.35 μm and Jsc in Excess of 34 mA cm-2. *Adv. Mater.* **2018**, *30*.

(11) Ramade, J.; Qu, J.; Chu, A.; Gréboval, C.; Livache, C.; Goubet, N.; Martinez, B.; Vincent, G.; Lhuillier, E. Potential of Colloidal Quantum Dot Based Solar Cells for Near-Infrared Active Detection. *ACS Photonics* **2020**, *7*, 272–278.

(12) Pradhan, S.; Di Stasio, F.; Bi, Y.; Gupta, S.; Christodoulou, S.; Stavrinadis, A.; Konstantatos, G. High-efficiency colloidal quantum dot infrared light-emitting diodes via engineering at the supra-nanocrystalline level. *Nat. Nanotechnol.* **2019**, *14*, 72–79.

(13) Qu, J.; Rastogi, P.; Gréboval, C.; Lagarde, D.; Chu, A.; Dabard, C.; Khalili, A.; Cruguel, H.; Robert, C.; Xu, X. Z.; Ithurria, S.; Silly, M. G.; Ferré, S.; Marie, X.; Lhuillier, E. Electroluminescence from HgTe Nanocrystals and Its Use for Active Imaging. *Nano Lett.* **2020**, *20*, 6185–6190.

(14) Vafaie, M.; Fan, J. Z.; Morteza Najarian, A.; Ouellette, O.; Sagar, L. K.; Bertens, K.; Sun, B.; García de Arquer, F. P.; Sargent, E. H. Colloidal quantum dot photodetectors with 10-ns response time and 80% quantum efficiency at 1,550 nm. *Matter* **2021**, *4*, 1042–1053.

(15) Rastogi, P.; Chu, A.; Dang, T. H.; Prado, Y.; Gréboval, C.; Qu, J.; Dabard, C.; Khalili, A.; Dandeu, E.; Fix, B.; Xu, X. Z.; Ithurria, S.; Vincent, G.; Gallas, B.; Lhuillier, E. Complex Optical Index of HgTe Nanocrystal Infrared Thin Films and Its Use for Short Wave Infrared Photodiode Design. *Adv. Opt. Mater.* **2021**, *9*, 2002066.

(16) Diroll, B. T.; Gaulding, E. A.; Kagan, C. R.; Murray, C. B. Spectrally-Resolved Dielectric Functions of Solution-Cast Quantum Dot Thin Films. *Chem. Mater.* **2015**, *27*, 6463–6469.

(17) Zhang, Z.; Thung, Y. T.; Chen, X.; Wang, L.; Fan, W.; Ding, L.; Sun, H. Study of Complex Optical Constants of Neat Cadmium Selenide Nanoplatelets Thin Films by Spectroscopic Ellipsometry. *J. Phys. Chem. Lett.* **2021**, *12*, 191–198.

(18) Moreels, I.; Kruschke, D.; Glas, P.; Tomm, J. W. The dielectric function of PbS quantum dots in a glass matrix. *Opt. Mater. Express* **2012**, *2*, 496–500.

(19) Grinolds, D. D. W.; Brown, P. R.; Harris, D. K.; Bulovic, V.; Bawendi, M. G. Quantum-dot size and thin-film dielectric constant: Precision measurement and disparity with simple models. *Nano Lett.* **2015**, *15*, 21–26.

(20) Georgitzikis, E.; Malinowski, P. E.; Maes, J.; Hadipour, A.; Hens, Z.; Heremans, P.; Cheyns,

D. Optimization of Charge Carrier Extraction in Colloidal Quantum Dots Short-Wave Infrared Photodiodes through Optical Engineering. *Adv. Funct. Mater.* **2018**, *28*, 1804502.
(21) Georgitzikis, E.; Genoe, J.; Heremans, P.; Cheyns, D. Carrier Mobility, Lifetime, and Diffusion Length in Optically Thin Quantum Dot Semiconductor Films. *ACS Appl. Mater. Interfaces* **2020**, *12*, 30565–30571.
(22) Moreels, I.; Lambert, K.; Smeets, D.; De Muynck, D.; Nollet, T.; Martins, J. C.; Vanhaecke, F.; Vantomme, A.; Delerue, C.; Allan, G.; Hens, Z. Size-dependent optical properties of colloidal PbS quantum dots. *ACS Nano* **2009**, *3*, 3023–3030.
(23) Moreels, I.; Allan, G.; De Geyter, B.; Wirtz, L.; Delerue, C.; Hens, Z. Dielectric function of colloidal lead chalcogenide quantum dots obtained by a Kramers-Krönig analysis of the absorbance spectrum. *Phys. Rev. B - Condens. Matter Mater. Phys.* **2010**, *81*, 1–7.
(24) Alves-Santos, M.; Di Felice, R.; Goldoni, G. Dielectric functions of semiconductor nanoparticles from the optical absorption spectrum: The case of CdSe and CdS. *J. Phys. Chem. C* **2010**, *114*, 3776–3780.
(25) Hens, Z.; Moreels, I. Light absorption by colloidal semiconductor quantum dots. *J. Mater. Chem.* **2012**, *22*, 10406–10415.
(26) Yu, P.; Beard, M. C.; Ellingson, R. J.; Fernere, S.; Curtis, C.; Drexler, J.; Luiszer, F.; Nozik, A. J. Absorption cross-section and related optical properties of colloidal InAs quantum dots. *J. Phys. Chem. B* **2005**, *109*, 7084–7087.
(27) Leatherdale, C. A.; Woo, W. K.; Mikulec, F. V.; Bawendi, M. G. On the absorption cross section of CdSe nanocrystal quantum dots. *J. Phys. Chem. B* **2002**, *106*, 7619–7622.
(28) Moreels, I.; Lambert, K.; De Muynck, D.; Vanhaecke, F.; Poelman, D.; Martins, J. C.; Allan, G.; Hens, Z. Composition and size-dependent extinction coefficient of colloidal PbSe quantum dots. *Chem. Mater.* **2007**, *19*, 6101–6106.
(29) Woo, H. C.; Choi, J. W.; Lee, J.-S.; Lee, C.-L. Determination of complex dielectric function of CH 3 NH 3 PbBr 3 perovskite cubic colloidal quantum dots by modified iterative matrix inversion method . *Opt. Express* **2019**, *27*, 20098.
(30) Sandeep, C. S. S.; Azpiroz, J. M.; Evers, W. H.; Boehme, S. C.; Moreels, I.; Kinge, S.; Siebbeles, L. D. A.; Infante, I.; Houtepen, A. J. Epitaxially connected PbSe quantum-dot films: Controlled neck formation and optoelectronic properties. *ACS Nano* **2014**, *8*, 11499–11511.
(31) Dement, D. B.; Puri, M.; Ferry, V. E. Determining the Complex Refractive Index of Neat CdSe/CdS Quantum Dot Films. *J. Phys. Chem. C* **2018**, *122*, 21557–21568.
(32) Agrawal, V. V.; Varghese, N.; Kulkarni, G. U.; Rao, C. N. R. Effects of changes in the interparticle separation induced by alkanethiols on the surface plasmon band and other properties of nanocrystalline gold films. *Langmuir* **2008**, *24*, 2494–2500.
(33) Moreels, I.; Justo, Y.; De Geyter, B.; Haustraete, K.; Martins, J. C.; Hens, Z. Size-Tunable, Bright, and Stable PbS Quantum Dots: A Surface Chemistry Study. *ACS Nano* **2011**, *5*, 2004–2012.
(34) Weidman, M. C.; Yager, K. G.; Tisdale, W. A. Interparticle spacing and structural ordering in superlattice pbs nanocrystal solids undergoing ligand exchange. *Chem. Mater.* **2015**, *27*, 474–482.
(35) Markel, V. A. Introduction to the Maxwell Garnett approximation: tutorial. *J. Opt. Soc. Am. A* **2016**, *33*, 1244.
(36) Choy, T. C. *Effective Medium Theory*; Oxford University Press, 2015.
(37) Chu, A.; Martinez, B.; Ferré, S.; Noguier, V.; Gréboval, C.; Livache, C.; Qu, J.; Prado, Y.; Casaretto, N.; Goubet, N.; Cruguel, H.; Dudy, L.; Silly, M. G.; Vincent, G.; Lhuillier, E. HgTe Nanocrystals for SWIR Detection and Their Integration up to the Focal Plane Array. *ACS Appl. Mater. Interfaces* **2019**, *11*, 33116–33123.
(38) Fan, J. Z.; Vafaie, M.; Bertens, K.; Sytnyk, M.; Pina, J. M.; Sagar, L. K.; Ouellette, O.; Proppe, A. H.; Rasouli, A. S.; Gao, Y.; Baek, S.-W.; Chen, B.; Laquai, F.; Hoogland, S.; Arquer, F. P. G. de; Heiss, W.; Sargent, E. H. Micron Thick Colloidal Quantum Dot Solids. *Nano Lett.* **2020**, *20*, 5284–5291.
(39) Chu, A.; Gréboval, C.; Goubet, N.; Martinez, B.; Livache, C.; Qu, J.; Rastogi, P.; Bresciani, F. A.; Prado, Y.; Suffit, S.; Ithurria, S.; Vincent, G.; Lhuillier, E. Near Unity Absorption in Nanocrystal Based Short Wave Infrared Photodetectors Using Guided Mode Resonators.

ACS Photonics **2019**, *6*, 2553–2561.
(40) Maniyara, R. A.; Graham, C.; Paulillo, B.; Bi, Y.; Chen, Y.; Herranz, G.; Baker, D. E.; Mazumder, P.; Konstantatos, G.; Pruneri, V. Highly transparent and conductive ITO substrates for near infrared applications. *APL Mater.* **2021**, *9*, 021121.
(41) Gréboval, C.; Noumbé, U. N.; Chu, A.; Prado, Y.; Khalili, A.; Dabard, C.; Dang, T. H.; Colis, S.; Chaste, J.; Ouerghi, A.; Dayen, J.-F.; Lhuillier, E. Gate tunable vertical geometry phototransistor based on infrared HgTe nanocrystals. *Appl. Phys. Lett.* **2020**, *117*, 251104.
(42) Tang, X.; Chen, M.; Kamath, A.; Ackerman, M. M.; Guyot-Sionnest, P. Colloidal Quantum-Dots/Graphene/Silicon Dual-Channel Detection of Visible Light and Short-Wave Infrared. *ACS Photonics* **2020**, *7*, 1117–1121.
(43) Larciprete, M. C.; Albertoni, A.; Belardini, A.; Leahu, G.; Li Voti, R.; Mura, F.; Sibilia, C.; Nefedov, I.; Anoshkin, I. V.; Kauppinen, E. I.; Nasibulin, A. G. Infrared properties of randomly oriented silver nanowires. *J. Appl. Phys.* **2012**, *112*, 083503.
(44) Delerue, C. *Nanostructure- Theory and Modeling*; 2003.
(45) Murray, C. B.; Kagan, C. R.; Bawendi, M. G. Synthesis and Characterization of Monodisperse Nanocrystals and Close-Packed Nanocrystal Assemblies. *Annu. Rev. Mater. Sci.* **2000**, *30*, 545–610.
(46) Hugonin, J. P.; Lalanne, P. *Reticolo Software for Grating Analysis*; 2005.

Supporting information

Complex Optical Index of PbS Nanocrystal Thin Film and their Use for Short Wave Infrared Sensor Design

Bilal Chehaibou[1], Eva Izquierdo[2], Audrey Chu[2] Claire Abadie[3], Mariarosa Cavallo[2], Adrien Khalili[2], Tung Huu Dang[2], Charlie Gréboval[2], Xiang Zhen Xu[4], Sandrine Ithurria[4], Grégory Vincent[3], Bruno Gallas[2], Gabriel Mugny[5], Arthur Arnaud[6], Emmanuel Lhuillier[2*], Christophe Delerue[1]*

[1]Univ. Lille, CNRS, Centrale Lille, Univ. Polytechnique Hauts-de-France, Junia, UMR 8520 - IEMN, F-59000 Lille, France
[2]Sorbonne Université, CNRS - UMR 7588, Institut des NanoSciences de Paris, INSP, F-75005 Paris, France
[3]ONERA - The French Aerospace Lab, 6, chemin de la Vauve aux Granges, BP 80100, 91123 Palaiseau, France.
[4] Laboratoire de Physique et d'Etude des Matériaux, ESPCI-Paris, PSL Research University, Sorbonne Université Univ Paris 06, CNRS UMR 8213, 10 rue Vauquelin 75005 Paris, France.
[5]STMicroelectronics, 12 rue Jules Horowitz, 38019 Grenoble, France.
[6]STMicroelectronics, 850 rue J. Monnet, 38926 Crolles, France.

*To whom correspondence should be sent: el@insp.upmc.fr and christophe.delerue@iemn.fr

Contents

1. Material synthesis

PbS 1000 synthesis: In a three-neck flask, 300 mg of $PbCl_2$ +100µL of TOP and 7.5 mL of OLA are degassed, first at room temperature and then at 110 °C for 30 min. Meanwhile 30 mg of S powder are mixed with 7.5 mL of OLA until full dissolution and a clear orange solution is obtained. Then under N_2 at 80 °C, this solution of S is quickly added to the flask. After 30 s, the reaction is quickly quenched by addition of 1 mL of oleic acid and 9 mL of hexane. The nanocrystals (NCs) are precipitated with ethanol and redispersed in toluene. This washing step is repeated one more time. The solution is then centrifuged to remove the unstable phase. The supernatant is precipitated with methanol and redispersed in toluene. For TEM images and absorption spectroscopy, see Figure S 1a.

PbS 1100 synthesis: In a three-neck flask, 300 mg of $PbCl_2$ +100µL of TOP and 7.5 mL of OLA are degassed, first at room temperature and then at 110 °C for 30 min. Meanwhile 30 mg of S powder are mixed with 7.5 mL of OLA until full dissolution and a clear orange solution is obtained. Then under N_2 at 90 °C, this solution of S is quickly added to the flask. After 1 minute, the reaction is quickly quenched by addition of 1 mL of oleic acid and 9 mL of hexane. The NCs are precipitated with ethanol and redispersed in toluene. This washing step is repeated one more time. The solution is then centrifuged to remove the unstable phase. The supernatant is precipitated with methanol and redispersed in toluene. For TEM images and absorption spectroscopy, see Figure S 1b.

PbS 1200 synthesis: In a three-neck flask, 300 mg of $PbCl_2$ +100µL of TOP and 7.5 mL of OLA are degassed, first at room temperature and then at 110 °C for 30 min. Meanwhile 30 mg of S powder are mixed with 7.5 mL of OLA until full dissolution and a clear orange solution is obtained. Then under N_2 at 90 °C, this solution of S is quickly added to the flask. After 3 minutes, the reaction is quickly quenched by addition of 1 mL of oleic acid and 9 mL of hexane. The NCs are precipitated with ethanol and redispersed in toluene. This washing step is repeated one more time. The solution is then centrifuged to remove the unstable phase. The supernatant is precipitated with methanol and redispersed in toluene. For TEM images and absorption spectroscopy, see Figure S 1c.

PbS 1370 synthesis: In a three-neck flask, 300 mg of $PbCl_2$ and 7.5 mL of OLA are degassed, first at room temperature and then at 110 °C for 30 min. Meanwhile 30 mg of S powder are mixed with 7.5 mL of OLA until full dissolution and a clear orange solution is obtained. Then under N_2 at 110 °C, this solution of S is quickly added to the flask. After 3 minutes, the reaction is quickly quenched by addition of 1 mL of oleic acid and 9 mL of hexane. The NCs are precipitated with ethanol and redispersed in toluene. This washing step is repeated one more time. The solution is then centrifuged to remove the unstable phase. The supernatant is precipitated with methanol and redispersed in toluene. For TEM images and absorption spectroscopy, see Figure S 1d

PbS 1450 Synthesis*:* In a three-neck flask, 300 mg of $PbCl_2$ and 7.5 mL of OLA are degassed, first at room temperature and then at 110 °C for 30 min. Meanwhile 30 mg of S powder are mixed with 7.5 mL of OLA until full dissolution and a clear orange solution is obtained. Then under N_2 at 110°C, this solution of S is quickly added to the flask. After 15 minutes, the reaction is quickly quenched by addition of 1 mL of oleic acid and 9 mL of hexane. The NCs are precipitated with ethanol and redispersed in toluene. This washing step is repeated one more time. The solution is then centrifuged to remove the

unstable phase. The supernatant is precipitated with methanol and redispersed in toluene. For TEM images and absorption spectroscopy, see Figure S 1e

PbS 1550 Synthesis*:* In a three-neck flask, 300 mg of $PbCl_2$ and 7.5 mL of OLA are degassed, first at room temperature and then at 110 °C for 30 min. Meanwhile 30 mg of S powder are mixed with 7.5 mL of OLA until full dissolution and a clear orange solution is obtained. Then under N_2 at 150 °C, this solution of S is quickly added to the flask. After 15 minutes, the reaction is quickly quenched by addition of 1 mL of oleic acid and 9 mL of hexane. The NCs are precipitated with ethanol and redispersed in hexane. Again, the NCs are precipitated with ethanol and redispersed in hexane and a drop of OA. The cleaning is repeated a third time. Finally, the NCs in hexane are then centrifuged to remove the unstable phase. For TEM images and absorption spectroscopy, see Figure S 1f

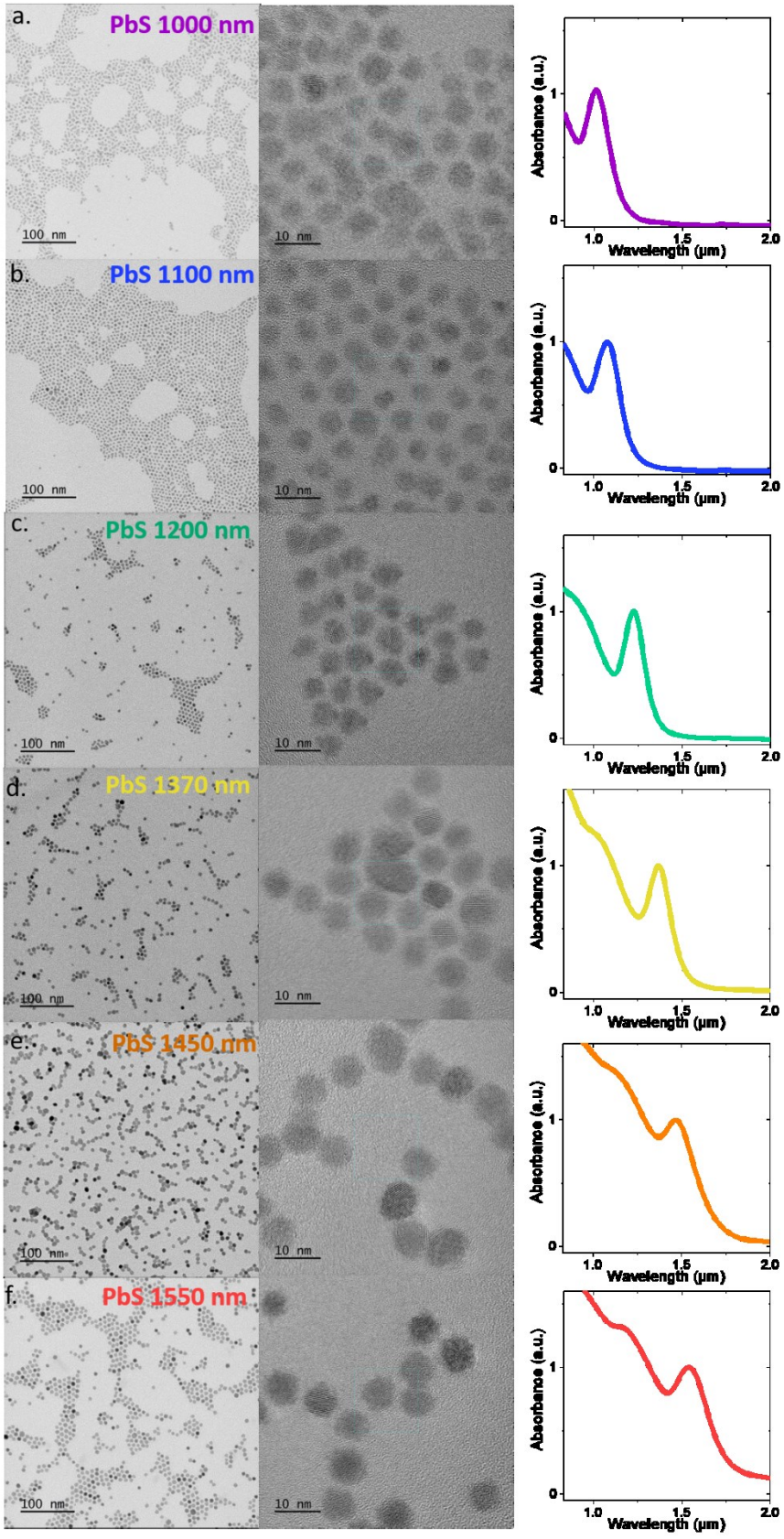

Figure S 1 On the left is a Transmission Electron microscopy (TEM) image of PbS NCs, in the middle is a high resolution TEM image and on the right absorption spectra for a. PbS 1000 nm, b. PbS 1100 nm, c. PbS 1200 nm, d. 1370 nm, e. PbS 1450 nm and f. PbS 1550 nm.

2. Ellipsometry measurements

2.1. Procedure to determine n and k from ellipsometry

The spectroscopic ellipsometry (SE) was performed on a variable angle spectroscopic ellipsometer (V-VASE from J.A. Wollam). The spectral range used was 0.45-2.100 µm. The measurements were performed at 3 angles of incidence: 50, 60 and 70 °.

Ellipsometry measures the change in the polarization state between the incident and the reflected light from a surface. The ellipsometric angles ψ and Δ are obtained from the complex reflectance ratio ρ as[1]:

$$\rho = \frac{(E_r/E_i)_p}{(E/E_i)_s} = \frac{r_p}{r_s} = \left|\frac{r_p}{r_s}\right| e^{i(\delta_p - \delta_s)} = \tan\psi\, e^{i\Delta}$$

Where r_p and r_s are the complex reflection coefficient of p and s polarized light, respectively, δ_p and δs the phase shifts at reflection for p and s polarizations, respectively.

The measured Ψ and Δ quantities were fitted to a multilayer model to determine the dielectric function of the NCs. The imaginary part of the dielectric function of the NCs (ε_2) was modelled as a linear summation of one Tauc-Lorentz oscillator and four Gaussian oscillators used to describe the absorption features, see Figure S2 (for an example of fit). We have tried different types of oscillators. The Tauc-Lorentz oscillator allowed reproducing very steep absorption edges without introducing residual absorption below the absorption edge, while ensuring the Kramers-Kronig consistency of the optical constants (like the Gaussian oscillators did). It seems to us that the decomposition presented here is the minimal efficient one.

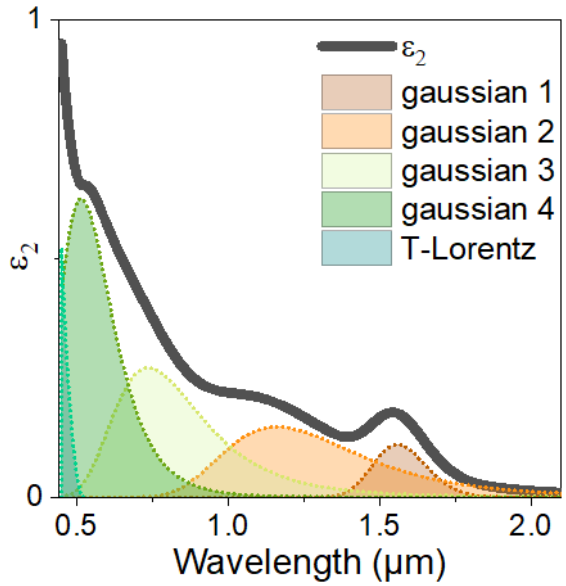

Figure S2 Example of a sum of oscillators used to fit ε_2, in the case of PbS 1550.

Each absorption feature in ε_2 is represented by a corresponding oscillator, whereas the real part ε_1 is calculated using Kramers-Kronig relations. We can derive the values of the optical constants n and k

$$\varepsilon_1 = n^2 - k^2$$

$$\varepsilon_2 = 2nk$$

n is the refractive index and k is the extinction coefficient.

The analysis of the data was performed using the software package WVASE32 to extract the optical constants of the NCs film. The final multilayer model defined here consists in a semi-infinite substrate with the optical constants of borosilicate glass (BK7) and a layer representing the NCs film with the oscillator model described. The thickness measured with the profilometer was used as the starting parameter in the model and was later fine-tuned when adjusting the parameters in the dispersion formula. First the adjustment was performed in the transparent region of the PbS film thus obtaining a reliable estimation of the thickness and the dielectric constant. Then, the fitting region was extended from the transparent region to the entire wavelength region.

The goodness of fit was determined using the unbiased merit function mean-squared error (MSE) which was minimized to best fit the model data (ψ,Δ) with experimental data (ψ,Δ), see Figure S 3.

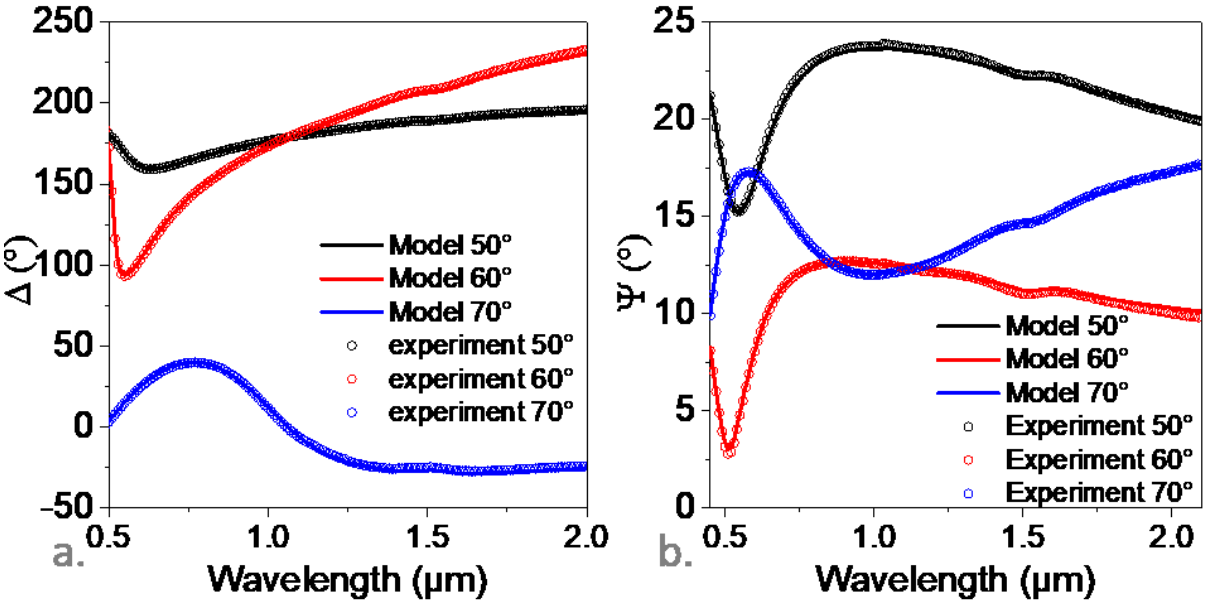

Figure S 3 Measured and fitted ellipsometry angles Δ (a.) and ψ (b.) as a function of the wavelength for three incident angles (50°, 60° and 70°) for the PbS 1550 sample.

2.2. Effect of particle size

For six different particle sizes (PbS 1000, 1100, 12000, 1370, 1450 and 1550 nm), we have measured the spectrally resolved complex optical index, see Figure S 4.

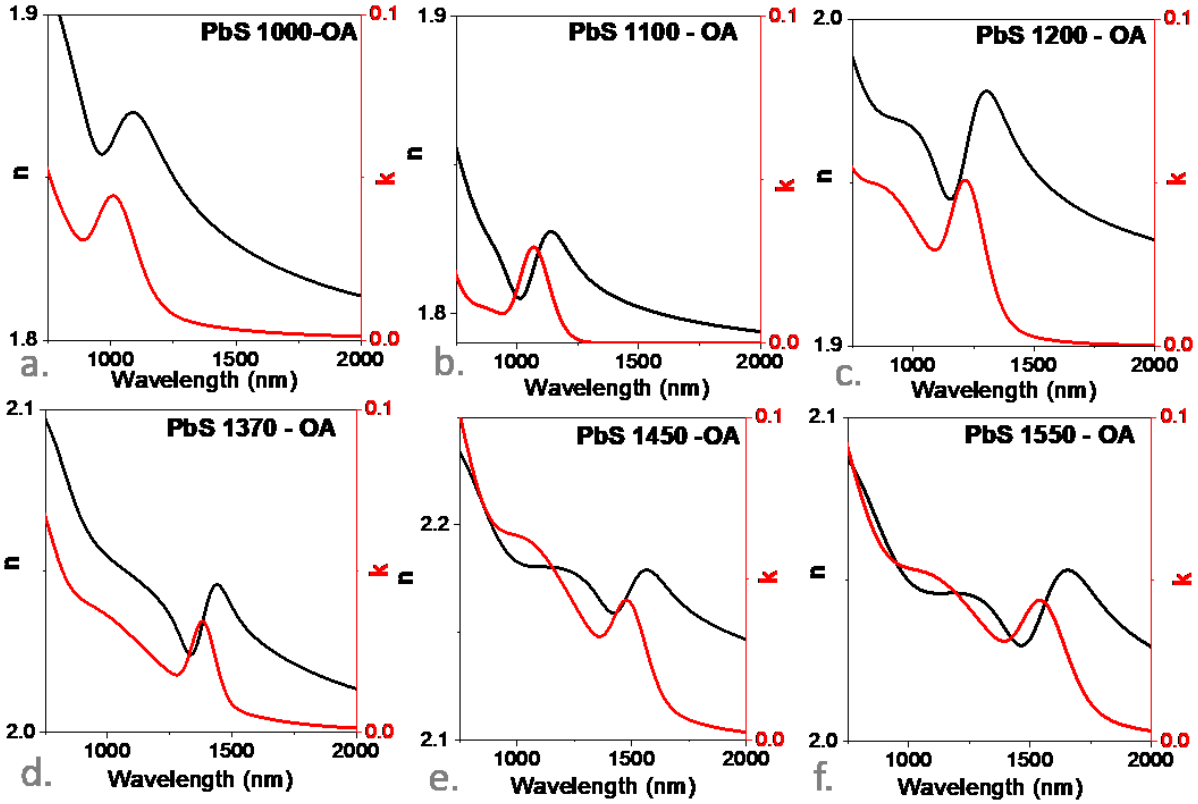

Figure S 4 Refractive index and extinction coefficient spectra for PbS NCs capped with oleic acid : a. for PbS 1000, b. for PbS 1100, c. for PbS 1200, d. for PbS 1370, e for PbS 1450 and f for PbS 1550.

2.3. Effect of surface chemistries

For three relevant particle sizes (1200, 1370 and 1550) we have conducted a ligand exchange from OA capping to EDT and NH_4I, see Figure S 5

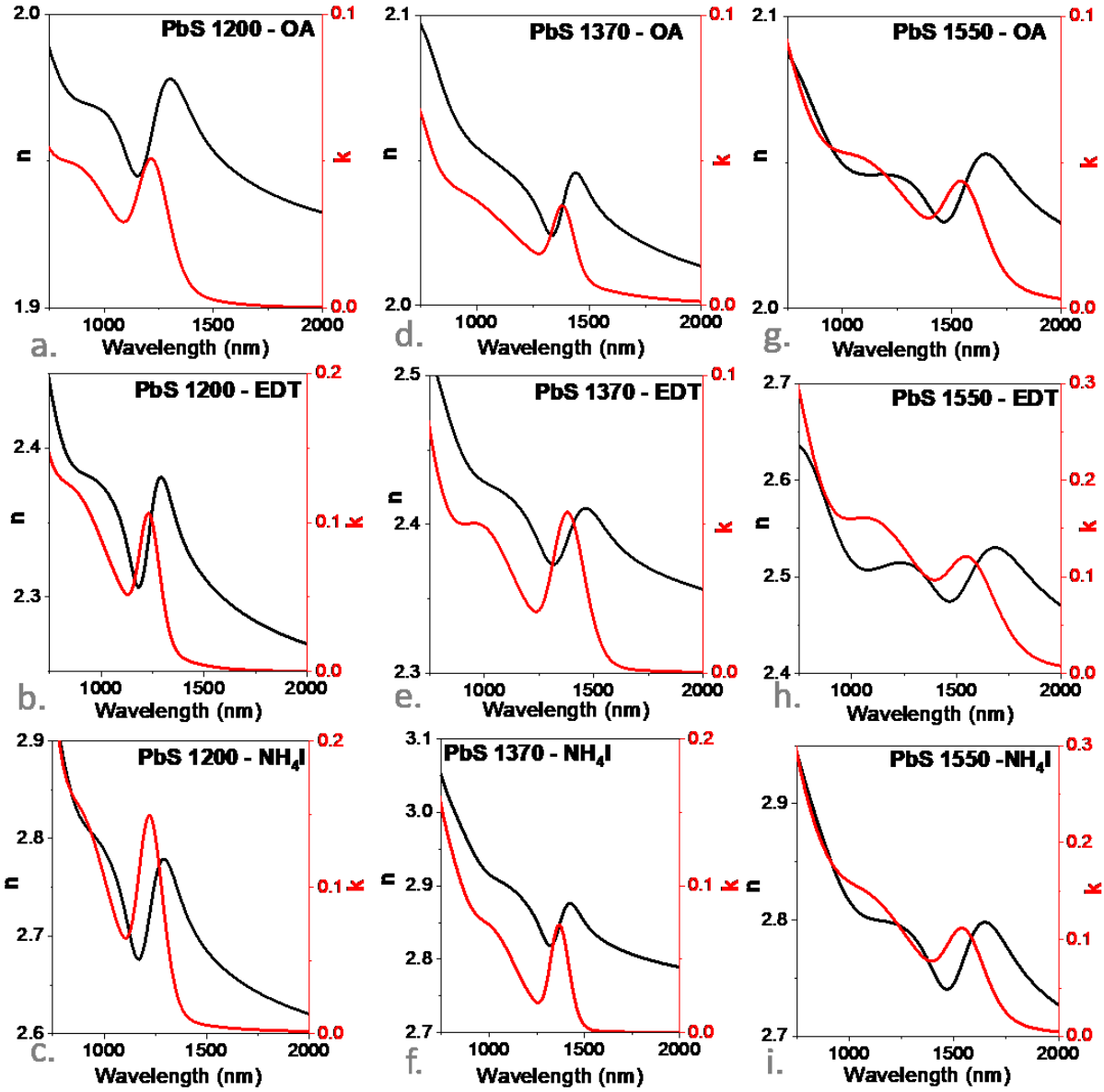

Figure S 5 Refractive index and extinction coefficient spectra for PbS 1200 capped with OA (a.), EDT (b.) and NH_4I (c.). Refractive index and extinction coefficient spectra for PbS 1370 capped with OA (e.), EDT (e.) and NH_4I (f.). Refractive index and extinction coefficient spectra for PbS 1550 capped with OA (g.), EDT (h.) and NH_4I (i.).

3. Electronic structure simulation and modelling of complex index

3.1. Tight-binding simulation

Table S 1 Top: first nearest-neighbour tight-binding (TB) parameters for PbS in $sp^3d^5s^*$ basis. The notation is that of Slater and Koster[2] (a =anion, c=cation). Δ is the spin-orbit coupling parameter.

Tight binding parameters for PbS

Intra-atomic terms :

$E_s^a = -13.84167$ eV	$E_s^c = -6.52122$ eV
$E_p^a = -1.16601$ eV	$E_p^c = 3.22618$ eV
$E_d^a = 10.10531$ eV	$E_d^c = 9.01082$ eV
$E_{s^*}^a = 98.98533$ eV	$E_{s^*}^c = 98.98533$ eV
$\Delta^a = 0.02467$ eV	$\Delta^c = 0.51967$ eV

First nearest neighbors interactions :

$E_{ss\sigma}(ac) = -0.35670$ eV	
$E_{s^*s^*\sigma}(ac) = 0.00000$ eV	
$E_{ss^*\sigma}(ac) = 0.00000$ eV	$E_{ss^*\sigma}(ca) = 0.00000$ eV
$E_{sp\sigma}(ac) = 0.11215$ eV	$E_{sp\sigma}(ca) = 0.93962$ eV
$E_{s^*p\sigma}(ac) = 0.00000$ eV	$E_{s^*p\sigma}(ca) = 0.00000$ eV
$E_{sd\sigma}(ac) = 0.00108$ eV	$E_{sd\sigma}(ca) = 0.02451$ eV
$E_{s^*d\sigma}(ac) = 0.00000$ eV	$E_{s^*d\sigma}(ca) = 0.00000$ eV
$E_{pp\sigma}(ac) = 2.02554$ eV	$E_{pp\pi}(ac) = -0.27864$ eV
$E_{pd\sigma}(ac) = -1.51112$ eV	$E_{pd\sigma}(ca) = -1.14642$ eV
$E_{pd\pi}(ac) = 0.50823$ eV	$E_{pd\pi}(ca) = 1.15990$ eV
$E_{dd\sigma}(ac) = -1.66943$ eV	$E_{dd\pi}(ac) = 0.00206$ eV
$E_{dd\delta}(ac) = 0.65772$ eV	

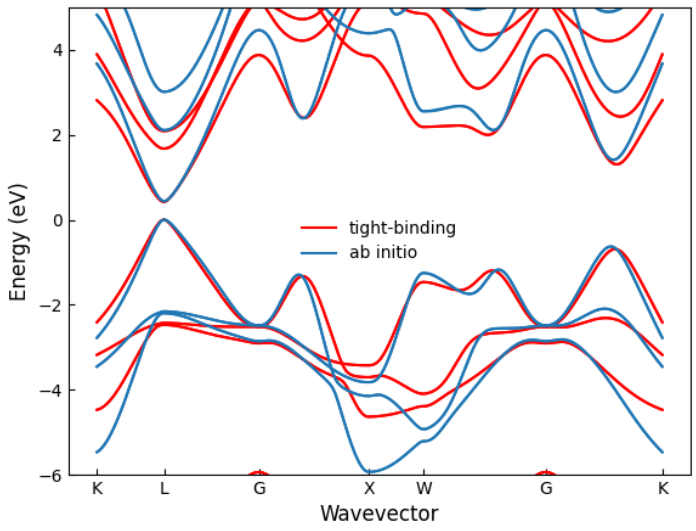

Figure S6 TB and ab initio band structure of bulk PbS, where the zero energy is the top of the valence band. The ab initio calculation has been performed using the Density Functional Theory (DFT) using the Heyd-Scuseria-Ernzerhof functional (HSE) and the Vienna ab initio simulation package (VASP; courtesy of Jing Li and Benoit Sklenard, CEA-LETI, Grenoble).

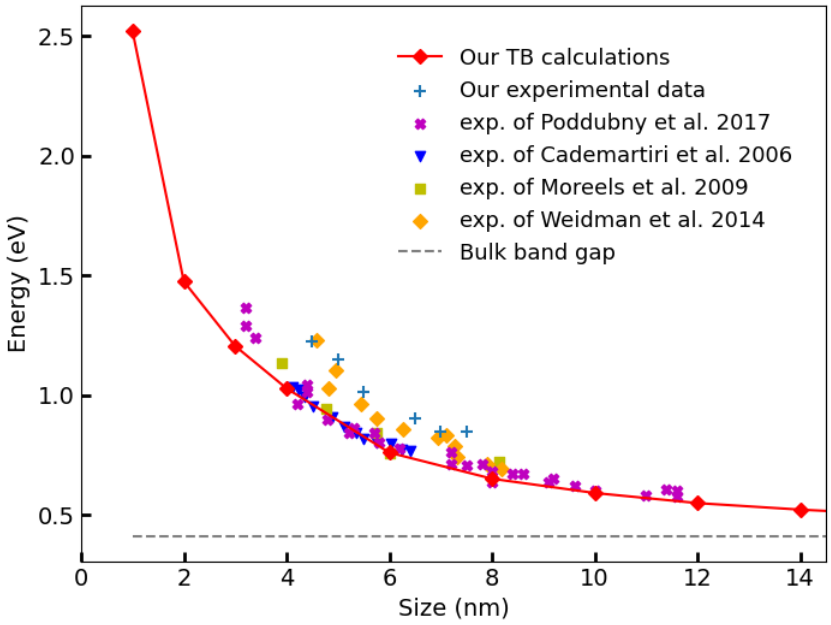

Figure S 7 Dependence between the PbS NCs bandgap and the particle size, calculated by tight-binding (red diamond) and measured in the present work (blue cross). Comparison from other works.[3–6]

We observed in Figure S 7 a constant shift between the TB size and those measured in TEM for a given exciton energy. Insofar, as the TB calculations agree with previous experimental data, we cannot explain the origin of these discrepancies.

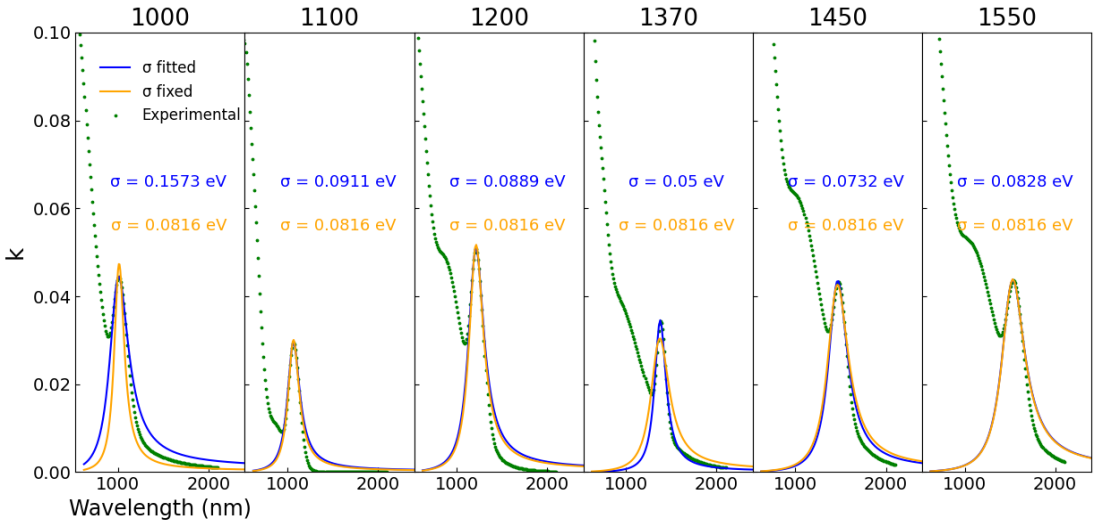

Figure S 8 Fitting the experimental excitonic peak of PbS 1000, 1100, 1200, 1370, 1450, and 1550 capped by oleic acid (green dot) with a Lorentzian at σ fixed (orange) and σ adjusted.

Figure S 8 shows that the broadening is quite similar for different PbS NCs films. Indeed, a Lorentzian for a fixed $\sigma = 0.0816$ eV well describes the exciton peak of the different films. Hence, the parameter

σ from equation 2 of the main document can be fitted once (here on PbS 1200) and transferred to the other films, removing one free parameter.

3.2. Maxwell Garnett vs Bruggeman

The Maxwell Garnett (MG) approximation is not symmetric. It is given by:

$$\frac{\varepsilon - \varepsilon_h}{\varepsilon + 2\varepsilon_h} = f_i \frac{\varepsilon_i - \varepsilon_h}{\varepsilon_i + 2\varepsilon_h}$$

with f_h and f_i the host and inclusion volume fraction; ε_i, ε_h, and ε the complex dielectric functions for the inclusion, the host, and the medium, respectively. The choice of which medium component (NC or ligand) entering the MG formula, either as the host or the inclusion, gives a different complex permittivity for the medium. The only possible distinction between components is based on an inclusion volume fraction much smaller than the host one. Thus, this theory is applicable only for dilute systems. The Bruggeman symmetric formulation is better suited for films where NCs can reach high volume fractions. The symmetry offered by the Bruggeman equation makes it possible to treat the medium components equally and thus overcome the Maxwell Garnett model restricted to dilute system and accessing denser composite mediums.

Both models (Figure S6) give the peaks shapes, positions, and magnitudes in good agreement with ellipsometry. The volume fractions extracted from MG are higher than those from Bruggeman. Even if MG is in accordance with experimental data, the theory is out of its validity limit when the host concentration is in the same order as the inclusion's concentration, as for NH_4I capping.

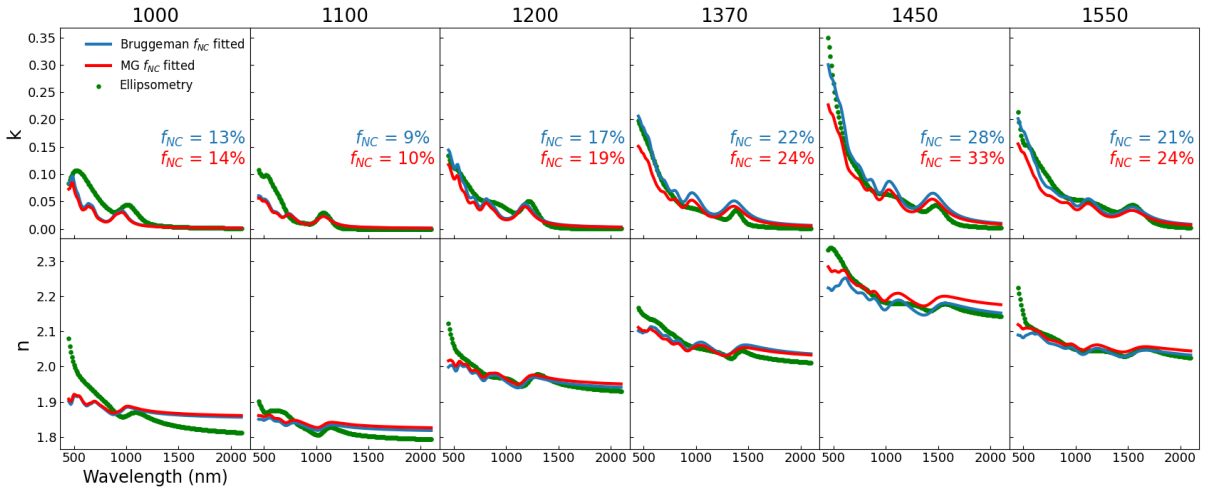

Figure S 9 Effect of particle size. Refractive index (n) and extinction coefficient (k) spectra for PbS 1000, 1100, 1200, 1370, 1450 and 1550 capped with OA. We compared the ellipsometry measurements (green dots), the Bruggeman (blue line) and the Maxwell Garnett (red line) approximations. The NC volume fractions (f_{NC}) obtained in the two approximations are indicated.

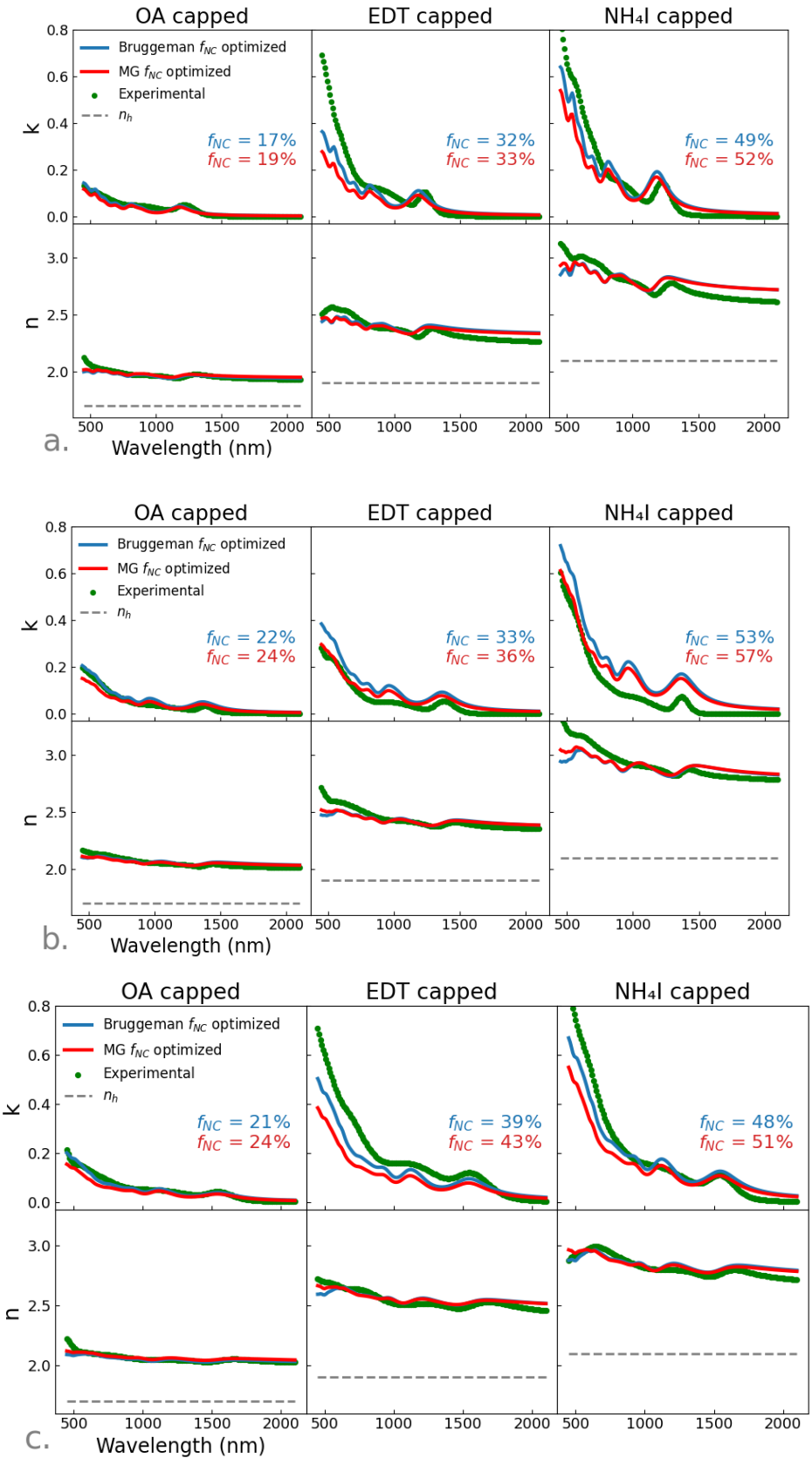

Figure S 10 Effect of surface chemistries. Refractive index (n) and extinction coefficient (k) spectra for PbS 1200 (a.), 1370 (b.) and 1550 (c.) capped with OA, EDT, and NH_4I. We compared the ellipsometry measurements (green dots), the Bruggeman (blue line) and the Maxwell Garnett (red line) approximations. The NC volume fractions (f_{NC}) obtained in the two approximations are indicated.

4. Electromagnetic simulation

4.1. Parameters for simulation

Electromagnetic simulations were implemented using a frequency-domain modal method known as the Rigorous Coupled Wave analysis (RCWA). We use RETICOLO,[7] a code written in MATLAB language. In this study, we have chosen 100 Fourier orders for the calculation.

We have chosen to model relevant stacks for IR sensing. The stack is made of glass/ITO (190 nm)/TiO2(120 nm)/PbS (n type, with NH4I capping and a tunable excitonic peak), PbS (p-type, capped with EDT and a 1200 nm excitonic peak)/Au (80 nm).
The last input needed for these calculations is the complex refractive index of each layer. For the ITO,[8] the TiO_2[9] and the gold[10] we used previously reported refractive index.

Again, it is worth pointing out that the p-type PbS layer is chosen to have a constant excitonic peak while the n type layer has a tunable excitonic peak. Indeed, the thiol capped PbS layer change from np type nature for a large excitonic peak (1200 nm and less) to n type for a wider excitonic peak.

The absorption map is deduced from the electric field at each point:

$$Loss = \frac{\pi}{\lambda}\int_S Im(\varepsilon(M))(\left|E_y\right|^2)dS\,, \qquad In\ TE\ polarisation$$

$$Loss = \frac{\pi}{\lambda}\int_S Im(\varepsilon(M))(|E_x|^2 + |E_z|^2)dS\,, \qquad In\ TM\ polarisation$$

Where S is a surface, $\varepsilon(M)$ is the permittivity at a point $M(x, y, z)$.
In the code the losses are calculated at each point of the map. There is a point every nanometer along the z-axis and a point every two nanometers along the x axis.

4.2. Tuning the relative thickness of n and p type layers in a PbS 1200 diode

One can notice that the spectral dependence of the refractive index is much weaker that in the case of the extinction coefficient. In Figure S 11, we address an important question which is whether the spectral dependence of the refractive index is a mandatory information to achieve accurate modelling. Conducting spectrally resolved measurement is experimentally challenging and sometimes unavailable at the laboratory level in the SWIR range. This explains why we have conducted absorption simulations for a diode at 1200, 1370 and 1550 nm when the full spectral dependence of the refractive index is considered and when it is replaced by its average value. For these three diodes, we have chosen a thickness which corresponds to a spectral overlap of a resonance with the exciton energy. We observe that overall modelling is only little affected by this approximation and in particular the properties close to the excitonic peak remains well reproduced.

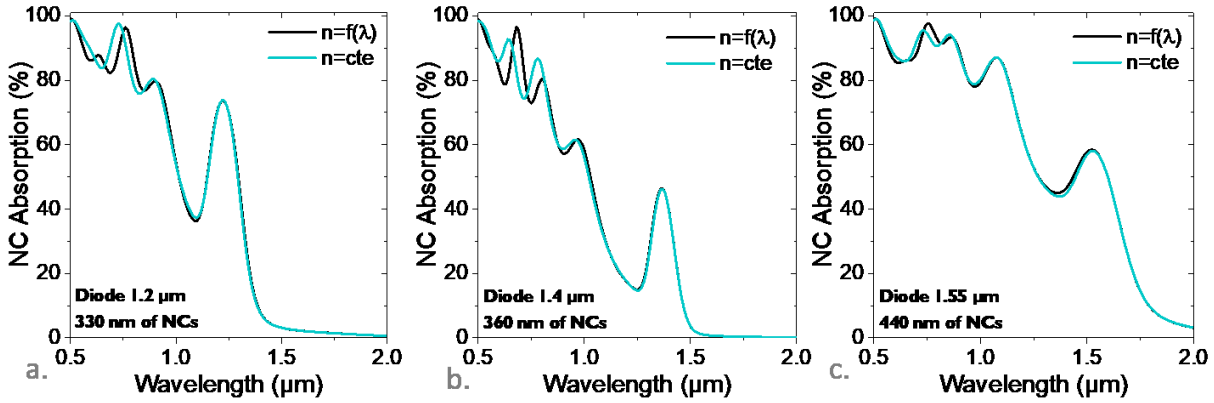

Figure S 11a. Absorption spectra within the NCs for a diode made of PbS 1200 for a spectrally dependant refractive index and for a refractive index averaged over the same spectral range. b. Absorption spectra within the NCs for a diode made of PbS 1370 for a spectrally dependant refractive index and for a refractive index averaged over the same spectral range. c. Absorption spectra within the NCs for a diode made of PbS for a spectrally dependant refractive index and for a refractive index averaged over the same spectral range.

4.3. Tuning the relative thickness of n and p type layers in PbS 1200 diode

In Figure S 12, we follow the absorption at the exciton as a function of the thicknesses of the thiol and I^- capped layers. We see that the resonance lines (yellow lines) follow exactly the iso thickness lines, meaning that the resonances are driven by the total thickness.

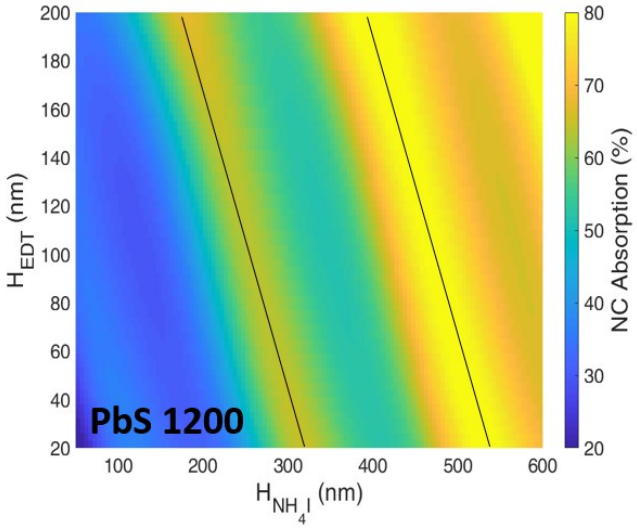

Figure S 12 Absorption within the NCs at the exciton for a diode made of PbS 1200 as a function of the thicknesses of the NH_4I capped PbS layer and the EDT capped PbS layer. The black lines are iso thickness lines.

4.4. Absorption with PbS 1370 diode sample

In Figure 6 of the main text, we show the absorption properties of a diode made of PbS 1200. Here, we expand this result to PbS 1370 (Figure S 13) and PbS 1550 (Figure S 14). Note that the diode stack is the same, except that the excitonic peak of the n type layer is tuned while keeping Iodide as a capping agent. Again, the p type layer remains made of PbS 1200 capped with EDT.

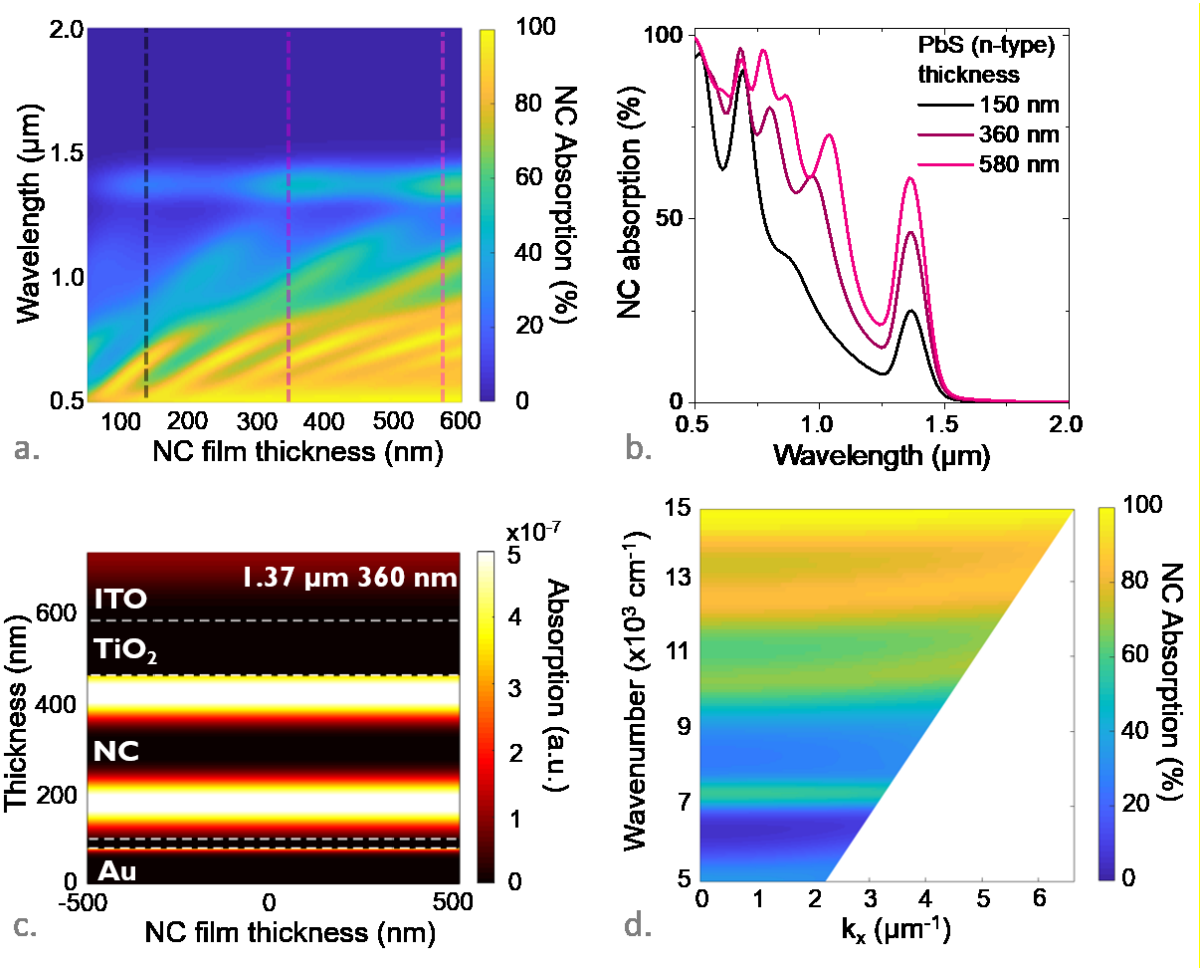

Figure S 13a. Absorption within the NCs for a diode made of PbS 1370 as a function of the wavelength and thickness of the n-type NH_4I capped PbS layer. b. Absorption spectra within the NCs for a diode made of PbS 1370 for two thicknesses of the n-type NH_4I capped PbS layer. c. Absorption spatial map for a diode made of PbS 1370. d. Dispersion relation (wavenumber as a function of k_x wavevector) for a diode made of PbS 1370. Exciton appears around 7000 cm^{-1}.

4.5. Absorption with PbS 1550 diode sample

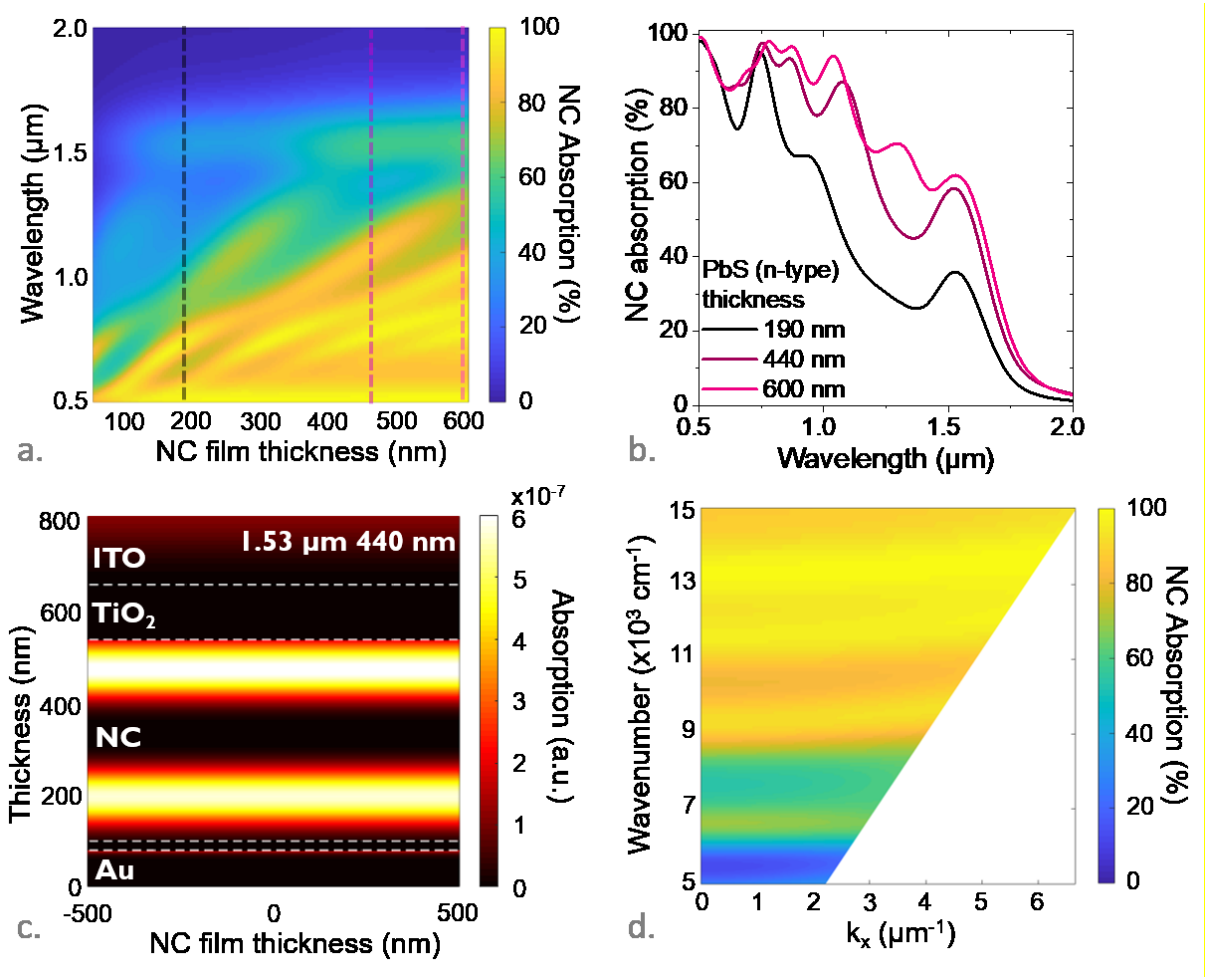

Figure S 14a. Absorption within the NCs for a diode made of PbS 1550 as a function of the wavelength and thickness of the n-type NH_4I capped PbS layer. b. Absorption spectra within the NCs for a diode made of PbS 1550 for two thicknesses of the n-type NH_4I capped PbS layer. c. Absorption spatial map for a diode made of PbS 1550. d. Dispersion relation (wavenumber as a function of k_x wavevector) for a diode made of PbS 1550. Exciton appears around 6400 cm^{-1}.

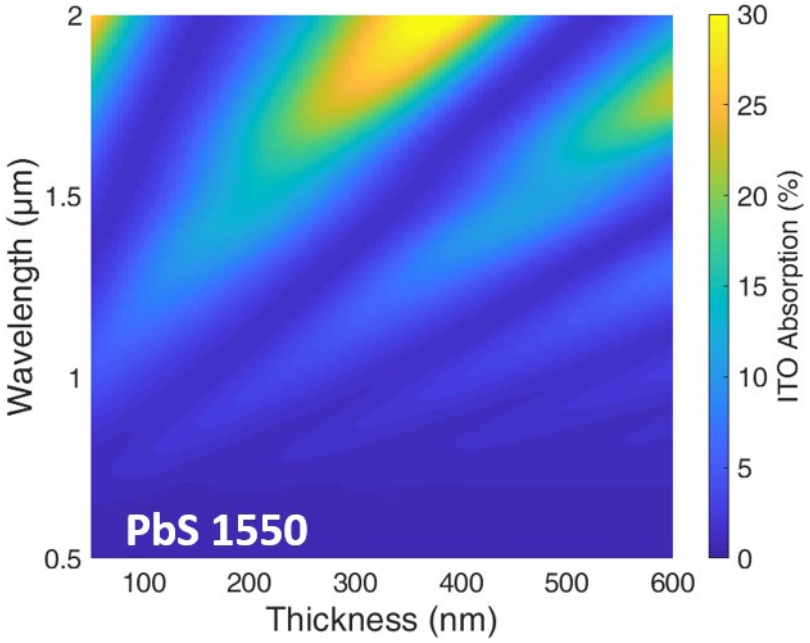

Figure S 15 . Absorption within the ITO for a diode made of PbS 1550 as a function of the wavelength and thickness of the n-type NH_4I capped PbS layer.

5. REFERENCES

(1) Fujiwara, H.; Collins, R. W. Spectroscopic Ellipsometry for Photovoltaics Volume 1: Fundamental Principles and Solar Cell Characterization. *Springer, Cham* **2018**.

(2) Koster, S. Simplified LCAO Method for the periodic potential problem. 1954.

(3) Poddubny, A. N.; Litvyak, V. M.; Nestoklon, M. O.; Cherbunin, R. V.; Golubkov, V. V.; Onushchenko, P. A.; Babkina, A. N.; Onushchenko, A. A.; Goupalov, S. V. Role of Valley Anisotropy in Optical Absorption of Monodisperse PbS Nanocrystals. *J. Phys. Chem. C* **2017**, *121*, 27766–27773.

(4) Weidman, M. C.; Beck, M. E.; Hoffman, R. S.; Prins, F.; Tisdale, W. A. Monodisperse, air-stable PbS nanocrystals via precursor stoichiometry control. *ACS Nano* **2014**, *8*, 6363–6371.

(5) Cademartiri, L.; Montanari, E.; Calestani, G.; Migliori, A.; Guagliardi, A.; Ozin, G. A. Size-dependent extinction coefficients of PbS quantum dots. *J. Am. Chem. Soc.* **2006**, *128*, 10337–10346.

(6) Moreels, I.; Lambert, K.; Smeets, D.; De Muynck, D.; Nollet, T.; Martins, J. C.; Vanhaecke, F.; Vantomme, A.; Delerue, C.; Allan, G.; Hens, Z. Size-dependent optical properties of colloidal PbS quantum dots. *ACS Nano* **2009**, *3*, 3023–3030.

(7) Hugonin, J.-P.; Lalanne, P. Reticolo software for grating analysis. 2005.

(8) Holman, Z. C.; Filipic, M.; Descoeudres, A.; De Wolf, S.; Smole, F.; Topic, M.; Ballif, C. Infrared light management in high-efficiency silicon heterojunction and rear-passivated solar cells. *J. Appl. Phys.* **2013**, *113*, 013107.

(9) Ratzsch, S.; Kley, E.-B.; Tuennermann, A.; Szeghalmi, A. Influence of the oxygen plasma parameters on the atomic layer deposition of titanium dioxide. *Nanotechnology* **2015**, *26*, 024003.

(10) Olmon, R. L.; Slovick, B.; Johnson, T. W.; Shelton, D.; Oh, S.-H.; Boreman, G. D.; Raschke, M. B. Optical dielectric function of gold. *Phys. Rev. B* **2012**, *86*, 235147.

6. Experimental data for the complex optical index

Ellipsometry measurement data (n,k) versus wavelength (nm) (Column 1 in wavelength in nm, column 2 is *n* column 3 is *k*) for the materials studied in the present work, see Figure S 4 and Figure S 5.

6.1. PbS 1000 - OA capping

450	2.08016	0.08326	920	1.86275	0.03283
460	2.05879	0.08939	930	1.8606	0.03421
470	2.04123	0.09461	940	1.85893	0.03585
480	2.02678	0.0989	950	1.8578	0.03763
490	2.01485	0.10224	960	1.85725	0.03942
500	2.00495	0.10467	970	1.85726	0.04111
510	1.99667	0.10625	980	1.85779	0.04255
520	1.98968	0.10704	990	1.85877	0.04364
530	1.9837	0.10711	1000	1.8601	0.0443
540	1.97852	0.10655	1010	1.86165	0.04447
550	1.97394	0.10545	1020	1.86331	0.04414
560	1.96984	0.10387	1030	1.86495	0.04331
570	1.96608	0.10191	1040	1.86647	0.04203
580	1.96259	0.09962	1050	1.86779	0.04036
590	1.95929	0.09707	1060	1.86883	0.03837
600	1.95613	0.09433	1070	1.86956	0.03615
610	1.95306	0.09143	1080	1.86996	0.03377
620	1.95006	0.08844	1090	1.87002	0.03133
630	1.94711	0.08537	1100	1.86977	0.02887
640	1.94418	0.08228	1110	1.86923	0.02648
650	1.94127	0.07918	1120	1.86843	0.02417
660	1.93837	0.0761	1130	1.86742	0.02201
670	1.93548	0.07306	1140	1.86623	0.02
680	1.93259	0.07008	1150	1.8649	0.01816
690	1.92971	0.06716	1160	1.86348	0.0165
700	1.92683	0.06431	1170	1.86199	0.01501
710	1.92396	0.06155	1180	1.86047	0.01368
720	1.92109	0.05888	1190	1.85893	0.01252
730	1.91824	0.05631	1200	1.85741	0.01149
740	1.91539	0.05383	1210	1.85591	0.0106
750	1.91255	0.05144	1220	1.85444	0.00982
760	1.90972	0.04916	1230	1.85302	0.00914
770	1.9069	0.04697	1240	1.85165	0.00855
780	1.90408	0.04488	1250	1.85033	0.00803
790	1.90127	0.04288	1260	1.84906	0.00758
800	1.89844	0.04098	1270	1.84785	0.00718
810	1.89559	0.03918	1280	1.84668	0.00683
820	1.89271	0.03748	1290	1.84557	0.00652
830	1.88979	0.03591	1300	1.84451	0.00624
840	1.8868	0.03449	1310	1.84349	0.00599
850	1.88376	0.03323	1320	1.84251	0.00576
860	1.88065	0.0322	1330	1.84157	0.00555
870	1.87749	0.03142	1340	1.84068	0.00536
880	1.87431	0.03095	1350	1.83981	0.00518
890	1.87117	0.03084	1360	1.83898	0.00502
900	1.86813	0.03111	1370	1.83818	0.00486
910	1.86529	0.03178	1380	1.83741	0.00472

1390	1.83666	0.00458	1750	1.81978	0.00196
1400	1.83594	0.00445	1760	1.81948	0.00193
1410	1.83524	0.00432	1770	1.81919	0.00189
1420	1.83457	0.00421	1780	1.81889	0.00185
1430	1.83392	0.00409	1790	1.81861	0.00182
1440	1.83328	0.00398	1800	1.81833	0.00178
1450	1.83266	0.00388	1810	1.81806	0.00175
1460	1.83206	0.00378	1820	1.81779	0.00172
1470	1.83148	0.00368	1830	1.81752	0.00169
1480	1.83092	0.00359	1840	1.81726	0.00166
1490	1.83036	0.0035	1850	1.81701	0.00163
1500	1.82983	0.00341	1860	1.81676	0.0016
1510	1.8293	0.00333	1870	1.81651	0.00157
1520	1.82879	0.00325	1880	1.81627	0.00154
1530	1.8283	0.00317	1890	1.81603	0.00152
1540	1.82781	0.0031	1900	1.8158	0.00149
1550	1.82734	0.00302	1910	1.81557	0.00146
1560	1.82688	0.00295	1920	1.81534	0.00144
1570	1.82642	0.00288	1930	1.81512	0.00142
1580	1.82598	0.00282	1940	1.81491	0.00139
1590	1.82555	0.00275	1950	1.81469	0.00137
1600	1.82513	0.00269	1960	1.81448	0.00135
1610	1.82472	0.00263	1970	1.81427	0.00133
1620	1.82432	0.00258	1980	1.81407	0.0013
1630	1.82392	0.00252	1990	1.81387	0.00128
1640	1.82354	0.00247	2000	1.81367	0.00126
1650	1.82316	0.00241	2010	1.81348	0.00124
1660	1.82279	0.00236	2020	1.81329	0.00122
1670	1.82243	0.00231	2030	1.8131	0.00121
1680	1.82207	0.00226	2040	1.81292	0.00119
1690	1.82172	0.00222	2050	1.81274	0.00117
1700	1.82138	0.00217	2060	1.81256	0.00115
1710	1.82105	0.00213	2070	1.81238	0.00113
1720	1.82072	0.00209	2080	1.81221	0.00112
1730	1.8204	0.00204	2090	1.81204	0.0011
1740	1.82009	0.002	2100	1.81187	0.00108

6.2. PbS 1100 - OA capping

450	1.90124	0.10786	950	1.81449	0.00937
460	1.89342	0.10298	960	1.81239	0.00991
470	1.88634	0.09956	970	1.81031	0.01088
480	1.8801	0.09742	980	1.80837	0.01232
490	1.87481	0.09648	990	1.80676	0.01424
500	1.87073	0.0967	1000	1.80563	0.01656
510	1.86865	0.09798	1010	1.80512	0.01916
520	1.86896	0.09843	1020	1.80535	0.02185
530	1.87017	0.09755	1030	1.80634	0.02442
540	1.87163	0.09559	1040	1.80804	0.02663
550	1.87299	0.0928	1050	1.81033	0.0283
560	1.87406	0.08946	1060	1.81302	0.02929
570	1.87474	0.08581	1070	1.81591	0.02952
580	1.87507	0.08205	1080	1.81878	0.02898
590	1.87513	0.07832	1090	1.82142	0.02776
600	1.87501	0.0747	1100	1.82369	0.02595
610	1.87483	0.07117	1110	1.82548	0.02372
620	1.87465	0.06768	1120	1.82672	0.02121
630	1.87449	0.06416	1130	1.82743	0.01858
640	1.8743	0.06053	1140	1.82762	0.01597
650	1.87403	0.05675	1150	1.82737	0.01347
660	1.87357	0.05281	1160	1.82675	0.01118
670	1.87285	0.04875	1170	1.82584	0.00913
680	1.8718	0.04464	1180	1.82472	0.00734
690	1.87039	0.04056	1190	1.82348	0.00583
700	1.86862	0.0366	1200	1.82217	0.00457
710	1.8665	0.03285	1210	1.82084	0.00355
720	1.8641	0.02937	1220	1.81953	0.00273
730	1.86146	0.0262	1230	1.81826	0.00209
740	1.85866	0.02339	1240	1.81706	0.00159
750	1.85575	0.02094	1250	1.81593	0.0012
760	1.85281	0.01885	1260	1.81487	9.12783E-4
770	1.84988	0.0171	1270	1.81389	6.95293E-4
780	1.84702	0.01567	1280	1.81298	5.33404E-4
790	1.84426	0.01453	1290	1.81214	4.13583E-4
800	1.84164	0.01364	1300	1.81136	3.25195E-4
810	1.83918	0.01295	1310	1.81063	2.60044E-4
820	1.83689	0.01243	1320	1.80995	2.11912E-4
830	1.83478	0.01204	1330	1.80931	1.76156E-4
840	1.83283	0.01172	1340	1.80872	1.49351E-4
850	1.83104	0.01146	1350	1.80816	1.28998E-4
860	1.82937	0.01121	1360	1.80763	1.13294E-4
870	1.82781	0.01096	1370	1.80713	1.00946E-4
880	1.82631	0.01068	1380	1.80665	9.10316E-5
890	1.82484	0.01038	1390	1.8062	8.28994E-5
900	1.82336	0.01005	1400	1.80576	7.6087E-5
910	1.82182	0.00972	1410	1.80535	7.02678E-5
920	1.82019	0.00943	1420	1.80495	6.521E-5
930	1.81843	0.00921	1430	1.80457	6.07482E-5
940	1.81652	0.00917	1440	1.8042	5.67634E-5

1450	1.80385	5.31689E-5	1780	1.79656	9.92046E-6
1460	1.80351	4.99005E-5	1790	1.79642	9.50831E-6
1470	1.80318	4.69098E-5	1800	1.79628	9.11675E-6
1480	1.80287	4.41594E-5	1810	1.79614	8.74459E-6
1490	1.80256	4.16201E-5	1820	1.79601	8.39074E-6
1500	1.80226	3.92681E-5	1830	1.79588	8.05414E-6
1510	1.80198	3.7084E-5	1840	1.79575	7.73383E-6
1520	1.8017	3.50515E-5	1850	1.79562	7.4289E-6
1530	1.80143	3.31568E-5	1860	1.7955	7.13849E-6
1540	1.80117	3.13878E-5	1870	1.79538	6.86182E-6
1550	1.80091	2.9734E-5	1880	1.79526	6.59812E-6
1560	1.80067	2.81861E-5	1890	1.79514	6.34669E-6
1570	1.80042	2.67356E-5	1900	1.79503	6.10688E-6
1580	1.80019	2.53753E-5	1910	1.79492	5.87806E-6
1590	1.79996	2.40984E-5	1920	1.79481	5.65966E-6
1600	1.79974	2.28986E-5	1930	1.7947	5.45111E-6
1610	1.79953	2.17706E-5	1940	1.79459	5.25192E-6
1620	1.79932	2.07092E-5	1950	1.79449	5.06159E-6
1630	1.79911	1.97098E-5	1960	1.79439	4.87966E-6
1640	1.79891	1.87682E-5	1970	1.79429	4.70571E-6
1650	1.79872	1.78804E-5	1980	1.79419	4.53932E-6
1660	1.79853	1.70428E-5	1990	1.79409	4.38013E-6
1670	1.79834	1.62522E-5	2000	1.794	4.22776E-6
1680	1.79816	1.55055E-5	2010	1.7939	4.08188E-6
1690	1.79798	1.47998E-5	2020	1.79381	3.94217E-6
1700	1.79781	1.41325E-5	2030	1.79372	3.80832E-6
1710	1.79764	1.35012E-5	2040	1.79363	3.68005E-6
1720	1.79748	1.29037E-5	2050	1.79355	3.55709E-6
1730	1.79731	1.23379E-5	2060	1.79346	3.43918E-6
1740	1.79716	1.18018E-5	2070	1.79338	3.32607E-6
1750	1.797	1.12936E-5	2080	1.79329	3.21755E-6
1760	1.79685	1.08117E-5	2090	1.79321	3.1134E-6
1770	1.7967	1.03545E-5	2100	1.79313	3.0134E-6

6.3. PbS 1200 – EDT capping

450	2.5105	0.69297	950	2.38038	0.10486
460	2.52041	0.66511	960	2.37961	0.10181
470	2.53079	0.63793	970	2.37873	0.09863
480	2.54118	0.61046	980	2.37772	0.09535
490	2.55081	0.58218	990	2.37655	0.09198
500	2.55882	0.55303	1000	2.37522	0.08856
510	2.56448	0.52339	1010	2.3737	0.0851
520	2.5673	0.49394	1020	2.37198	0.08163
530	2.56715	0.46551	1030	2.37006	0.07817
540	2.56423	0.43903	1040	2.36791	0.07473
550	2.55915	0.41536	1050	2.36551	0.07134
560	2.55293	0.39524	1060	2.36285	0.06801
570	2.54741	0.3792	1070	2.35989	0.06476
580	2.54587	0.36482	1080	2.35656	0.06163
590	2.54559	0.34867	1090	2.3528	0.05867
600	2.54494	0.33154	1100	2.34853	0.05598
610	2.54343	0.31396	1110	2.34365	0.05374
620	2.54087	0.29634	1120	2.33812	0.05218
630	2.53721	0.27901	1130	2.33198	0.05166
640	2.53249	0.26221	1140	2.32543	0.05257
650	2.52677	0.24613	1150	2.31889	0.05527
660	2.52016	0.23092	1160	2.31299	0.06001
670	2.51278	0.21672	1170	2.30856	0.06675
680	2.50477	0.2036	1180	2.30642	0.07506
690	2.49626	0.19163	1190	2.30724	0.08416
700	2.4874	0.18085	1200	2.31135	0.09294
710	2.47835	0.17128	1210	2.31855	0.10023
720	2.46925	0.16289	1220	2.32821	0.10496
730	2.46025	0.15565	1230	2.33928	0.10647
740	2.45149	0.1495	1240	2.35058	0.1045
750	2.44307	0.14437	1250	2.36099	0.09932
760	2.4351	0.14015	1260	2.36959	0.09153
770	2.42767	0.13674	1270	2.37583	0.08196
780	2.42084	0.13402	1280	2.37949	0.07149
790	2.41465	0.13188	1290	2.38068	0.06095
800	2.40912	0.13018	1300	2.3797	0.05097
810	2.40425	0.12882	1310	2.37703	0.04201
820	2.40002	0.12769	1320	2.37314	0.0343
830	2.39641	0.12668	1330	2.36852	0.02792
840	2.39337	0.12571	1340	2.36354	0.02278
850	2.39085	0.12471	1350	2.35852	0.01876
860	2.38878	0.1236	1360	2.35364	0.01567
870	2.3871	0.12235	1370	2.34904	0.01332
880	2.38575	0.12091	1380	2.34478	0.01153
890	2.38466	0.11927	1390	2.34087	0.01017
900	2.38377	0.1174	1400	2.33729	0.00911
910	2.38302	0.11531	1410	2.33402	0.00827
920	2.38235	0.113	1420	2.33102	0.00758
930	2.38172	0.11047	1430	2.32826	0.007
940	2.38107	0.10776	1440	2.3257	0.0065

1450	2.32331	0.00606	1780	2.28152	8.0325E-4
1460	2.32106	0.00566	1790	2.28079	7.59355E-4
1470	2.31895	0.00529	1800	2.28008	7.18082E-4
1480	2.31695	0.00496	1810	2.27938	6.79261E-4
1490	2.31505	0.00465	1820	2.2787	6.42739E-4
1500	2.31324	0.00436	1830	2.27803	6.08369E-4
1510	2.31151	0.00409	1840	2.27738	5.76015E-4
1520	2.30985	0.00384	1850	2.27674	5.45551E-4
1530	2.30826	0.0036	1860	2.27612	5.16859E-4
1540	2.30673	0.00338	1870	2.27551	4.89828E-4
1550	2.30526	0.00317	1880	2.27492	4.64354E-4
1560	2.30384	0.00298	1890	2.27434	4.40341E-4
1570	2.30247	0.0028	1900	2.27377	4.17699E-4
1580	2.30114	0.00263	1910	2.27321	3.96344E-4
1590	2.29986	0.00247	1920	2.27266	3.76196E-4
1600	2.29862	0.00232	1930	2.27213	3.57182E-4
1610	2.29742	0.00219	1940	2.27161	3.39233E-4
1620	2.29626	0.00206	1950	2.27109	3.22284E-4
1630	2.29513	0.00193	1960	2.27059	3.06276E-4
1640	2.29404	0.00182	1970	2.2701	2.91151E-4
1650	2.29297	0.00171	1980	2.26962	2.76857E-4
1660	2.29194	0.00161	1990	2.26914	2.63344E-4
1670	2.29094	0.00152	2000	2.26868	2.50566E-4
1680	2.28997	0.00143	2010	2.26822	2.38479E-4
1690	2.28902	0.00135	2020	2.26778	2.27043E-4
1700	2.2881	0.00127	2030	2.26734	2.1622E-4
1710	2.2872	0.0012	2040	2.26691	2.05974E-4
1720	2.28632	0.00113	2050	2.26649	1.96271E-4
1730	2.28547	0.00107	2060	2.26608	1.8708E-4
1740	2.28464	0.00101	2070	2.26567	1.78371E-4
1750	2.28383	9.52508E-4	2080	2.26527	1.70118E-4
1760	2.28304	8.99628E-4	2090	2.26488	1.62293E-4
1770	2.28228	8.49943E-4	2100	2.2645	1.54872E-4

6.4. PbS 1200 – NH_4I capping

450	3.12573	0.85429	950	2.80316	0.13192
460	3.11536	0.80529	960	2.80066	0.12736
470	3.10242	0.76032	970	2.79799	0.12256
480	3.08687	0.71966	980	2.79509	0.11758
490	3.069	0.68405	990	2.79191	0.11247
500	3.04967	0.6544	1000	2.78842	0.10729
510	3.0305	0.63133	1010	2.78458	0.10207
520	3.01361	0.61469	1020	2.78036	0.09688
530	3.00113	0.60319	1030	2.77572	0.09175
540	2.99444	0.59454	1040	2.77061	0.08674
550	2.99368	0.58598	1050	2.76498	0.08192
560	2.99768	0.57502	1060	2.75876	0.07737
570	3.0043	0.56013	1070	2.75186	0.07322
580	3.0111	0.54103	1080	2.74423	0.06965
590	3.01603	0.51857	1090	2.73581	0.06692
600	3.01786	0.49434	1100	2.72665	0.06536
610	3.01637	0.47018	1110	2.71691	0.06536
620	3.01255	0.44755	1120	2.70693	0.06731
630	3.00731	0.42633	1130	2.69722	0.07151
640	3.00097	0.40695	1140	2.68849	0.07811
650	2.99436	0.38952	1150	2.68154	0.087
660	2.98818	0.37367	1160	2.6772	0.09775
670	2.98277	0.35879	1170	2.67611	0.10961
680	2.97814	0.34426	1180	2.67867	0.12155
690	2.97401	0.32958	1190	2.68487	0.13247
700	2.96997	0.31449	1200	2.69429	0.14126
710	2.96553	0.29894	1210	2.70617	0.14706
720	2.9603	0.2831	1220	2.71951	0.14932
730	2.95399	0.26727	1230	2.7332	0.14786
740	2.94649	0.25183	1240	2.74619	0.14288
750	2.93781	0.23715	1250	2.75763	0.13487
760	2.92811	0.22356	1260	2.76687	0.1245
770	2.91764	0.2113	1270	2.77355	0.11255
780	2.9067	0.20054	1280	2.77758	0.0998
790	2.89559	0.19133	1290	2.77904	0.08694
800	2.88465	0.18362	1300	2.77822	0.07455
810	2.87412	0.1773	1310	2.77548	0.06306
820	2.86424	0.1722	1320	2.77124	0.05274
830	2.85517	0.16812	1330	2.76592	0.04374
840	2.84699	0.16481	1340	2.75991	0.03609
850	2.83976	0.16206	1350	2.75352	0.02974
860	2.83346	0.15965	1360	2.74702	0.02456
870	2.82803	0.1574	1370	2.74062	0.0204
880	2.8234	0.15513	1380	2.73445	0.01713
890	2.81944	0.15271	1390	2.7286	0.01457
900	2.81605	0.15006	1400	2.7231	0.01258
910	2.81308	0.14711	1410	2.71798	0.01105
920	2.81043	0.14382	1420	2.71323	0.00986
930	2.80796	0.14019	1430	2.70883	0.00894
940	2.80557	0.13621	1440	2.70474	0.00821

1450	2.70094	0.00763	1780	2.63906	0.00256
1460	2.69741	0.00716	1790	2.638	0.0025
1470	2.6941	0.00677	1800	2.63697	0.00244
1480	2.691	0.00643	1810	2.63596	0.00239
1490	2.68808	0.00614	1820	2.63498	0.00233
1500	2.68532	0.00588	1830	2.63401	0.00228
1510	2.6827	0.00564	1840	2.63307	0.00223
1520	2.68021	0.00543	1850	2.63215	0.00218
1530	2.67783	0.00523	1860	2.63124	0.00214
1540	2.67556	0.00505	1870	2.63036	0.00209
1550	2.67339	0.00487	1880	2.62949	0.00205
1560	2.6713	0.00471	1890	2.62865	0.00201
1570	2.6693	0.00456	1900	2.62782	0.00196
1580	2.66736	0.00441	1910	2.627	0.00192
1590	2.6655	0.00428	1920	2.62621	0.00189
1600	2.6637	0.00415	1930	2.62543	0.00185
1610	2.66196	0.00402	1940	2.62466	0.00181
1620	2.66028	0.0039	1950	2.62391	0.00178
1630	2.65865	0.00379	1960	2.62317	0.00174
1640	2.65707	0.00368	1970	2.62245	0.00171
1650	2.65554	0.00358	1980	2.62174	0.00167
1660	2.65406	0.00348	1990	2.62105	0.00164
1670	2.65261	0.00338	2000	2.62037	0.00161
1680	2.65121	0.00329	2010	2.6197	0.00158
1690	2.64985	0.00321	2020	2.61904	0.00155
1700	2.64852	0.00312	2030	2.61839	0.00152
1710	2.64723	0.00304	2040	2.61776	0.0015
1720	2.64597	0.00297	2050	2.61714	0.00147
1730	2.64475	0.00289	2060	2.61653	0.00144
1740	2.64355	0.00282	2070	2.61592	0.00142
1750	2.64239	0.00275	2080	2.61533	0.00139
1760	2.64125	0.00269	2090	2.61475	0.00137
1770	2.64014	0.00262	2100	2.61418	0.00135

6.5. PbS 1200 – OA capping

450	2.12367	0.13349	950	1.96884	0.04334
460	2.10684	0.12596	960	1.96854	0.04231
470	2.09222	0.12056	970	1.96819	0.04121
480	2.07961	0.11667	980	1.96777	0.04007
490	2.0688	0.11386	990	1.96728	0.03889
500	2.05956	0.11191	1000	1.96668	0.03767
510	2.05182	0.11075	1010	1.96598	0.03644
520	2.046	0.11027	1020	1.96515	0.0352
530	2.04207	0.10908	1030	1.96417	0.03397
540	2.03886	0.10707	1040	1.96303	0.03279
550	2.03596	0.10455	1050	1.96171	0.03169
560	2.03319	0.10173	1060	1.96018	0.03072
570	2.03051	0.0988	1070	1.95845	0.02994
580	2.0279	0.09584	1080	1.95654	0.02943
590	2.02538	0.0929	1090	1.95447	0.02926
600	2.02297	0.09001	1100	1.95233	0.02952
610	2.02066	0.08714	1110	1.95022	0.03027
620	2.01844	0.08431	1120	1.94827	0.03155
630	2.01628	0.08148	1130	1.94663	0.03333
640	2.01416	0.07866	1140	1.94546	0.03558
650	2.01204	0.07585	1150	1.94491	0.03817
660	2.00988	0.07307	1160	1.94508	0.04095
670	2.00766	0.07035	1170	1.94603	0.04371
680	2.00537	0.06772	1180	1.94775	0.04626
690	2.003	0.06521	1190	1.95019	0.04839
700	2.00056	0.06286	1200	1.95321	0.04992
710	1.99807	0.0607	1210	1.95663	0.05073
720	1.99555	0.05875	1220	1.96027	0.05074
730	1.99303	0.05702	1230	1.96391	0.04996
740	1.99054	0.05552	1240	1.96737	0.04841
750	1.98812	0.05425	1250	1.97049	0.0462
760	1.9858	0.0532	1260	1.97314	0.04345
770	1.98361	0.05235	1270	1.97524	0.04029
780	1.98157	0.05168	1280	1.97675	0.03689
790	1.9797	0.05115	1290	1.97767	0.03337
800	1.97801	0.05075	1300	1.97804	0.02987
810	1.97651	0.05043	1310	1.97791	0.02648
820	1.97519	0.05017	1320	1.97734	0.02329
830	1.97405	0.04995	1330	1.97642	0.02034
840	1.97309	0.04972	1340	1.97523	0.01768
850	1.97229	0.04948	1350	1.97383	0.01532
860	1.97162	0.0492	1360	1.97229	0.01325
870	1.97108	0.04886	1370	1.97068	0.01146
880	1.97065	0.04846	1380	1.96904	0.00993
890	1.9703	0.04798	1390	1.96741	0.00864
900	1.97001	0.04741	1400	1.96581	0.00755
910	1.96976	0.04676	1410	1.96426	0.00664
920	1.96954	0.04603	1420	1.96278	0.00587
930	1.96932	0.04521	1430	1.96138	0.00524
940	1.96909	0.04431	1440	1.96005	0.00471

1450	1.9588	0.00426	1780	1.93836	5.99798E-4
1460	1.95762	0.00388	1790	1.93803	5.70498E-4
1470	1.95651	0.00356	1800	1.9377	5.42773E-4
1480	1.95546	0.00328	1810	1.93738	5.16531E-4
1490	1.95447	0.00304	1820	1.93706	4.91688E-4
1500	1.95354	0.00283	1830	1.93676	4.68163E-4
1510	1.95266	0.00264	1840	1.93646	4.45881E-4
1520	1.95182	0.00248	1850	1.93617	4.24772E-4
1530	1.95102	0.00232	1860	1.93588	4.0477E-4
1540	1.95027	0.00219	1870	1.9356	3.85811E-4
1550	1.94954	0.00206	1880	1.93533	3.67837E-4
1560	1.94885	0.00194	1890	1.93506	3.50793E-4
1570	1.94818	0.00183	1900	1.9348	3.34627E-4
1580	1.94755	0.00173	1910	1.93455	3.19289E-4
1590	1.94693	0.00164	1920	1.9343	3.04735E-4
1600	1.94634	0.00155	1930	1.93406	2.9092E-4
1610	1.94577	0.00146	1940	1.93382	2.77804E-4
1620	1.94522	0.00139	1950	1.93358	2.65348E-4
1630	1.94469	0.00131	1960	1.93335	2.53516E-4
1640	1.94418	0.00124	1970	1.93313	2.42275E-4
1650	1.94368	0.00118	1980	1.93291	2.31592E-4
1660	1.94319	0.00112	1990	1.93269	2.21437E-4
1670	1.94273	0.00106	2000	1.93248	2.11781E-4
1680	1.94227	0.001	2010	1.93227	2.02599E-4
1690	1.94183	9.52521E-4	2020	1.93207	1.93863E-4
1700	1.9414	9.03861E-4	2030	1.93187	1.85552E-4
1710	1.94099	8.57912E-4	2040	1.93168	1.77641E-4
1720	1.94058	8.14511E-4	2050	1.93148	1.7011E-4
1730	1.94019	7.73508E-4	2060	1.9313	1.62939E-4
1740	1.9398	7.34761E-4	2070	1.93111	1.5611E-4
1750	1.93943	6.98136E-4	2080	1.93093	1.49604E-4
1760	1.93907	6.63511E-4	2090	1.93075	1.43404E-4
1770	1.93871	6.30768E-4	2100	1.93058	1.37494E-4

6.6. PbS 1370 – EDT capping

450	2.71268	0.28164	940	2.43638	0.05038
460	2.69022	0.26712	950	2.43455	0.05043
470	2.66916	0.2557	960	2.43296	0.05041
480	2.64956	0.24727	970	2.43158	0.0503
490	2.63171	0.2419	980	2.43039	0.05007
500	2.61627	0.23978	990	2.42935	0.04972
510	2.60509	0.241	1000	2.42842	0.04923
520	2.60005	0.24139	1010	2.42759	0.0486
530	2.59758	0.23915	1020	2.42681	0.04783
540	2.59626	0.23482	1030	2.42607	0.04693
550	2.59532	0.22888	1040	2.42533	0.0459
560	2.59436	0.22174	1050	2.42458	0.04475
570	2.59312	0.21375	1060	2.42379	0.04349
580	2.59149	0.2052	1070	2.42294	0.04215
590	2.5894	0.19632	1080	2.42203	0.04073
600	2.58684	0.18731	1090	2.42104	0.03924
610	2.58385	0.1783	1100	2.41996	0.03771
620	2.58045	0.16942	1110	2.41878	0.03614
630	2.57669	0.16073	1120	2.41749	0.03456
640	2.57261	0.15231	1130	2.41609	0.03296
650	2.56828	0.14418	1140	2.41458	0.03138
660	2.56372	0.13638	1150	2.41294	0.02981
670	2.55898	0.12891	1160	2.41116	0.02828
680	2.55409	0.12179	1170	2.40923	0.0268
690	2.54907	0.11502	1180	2.40714	0.02539
700	2.54397	0.10859	1190	2.40487	0.02407
710	2.53878	0.1025	1200	2.4024	0.02289
720	2.53353	0.09675	1210	2.39973	0.0219
730	2.52824	0.09133	1220	2.39685	0.02115
740	2.5229	0.08625	1230	2.39378	0.02073
750	2.51754	0.08149	1240	2.39055	0.02071
760	2.51216	0.07707	1250	2.38723	0.02118
770	2.50678	0.07299	1260	2.38393	0.02222
780	2.5014	0.06925	1270	2.38078	0.02387
790	2.49606	0.06586	1280	2.37794	0.02615
800	2.49075	0.06283	1290	2.37558	0.02902
810	2.48552	0.06015	1300	2.37387	0.03238
820	2.48039	0.05782	1310	2.37297	0.03609
830	2.47539	0.05585	1320	2.37296	0.03996
840	2.47055	0.05421	1330	2.37391	0.04375
850	2.46591	0.05289	1340	2.37579	0.04723
860	2.46149	0.05188	1350	2.3785	0.05018
870	2.45732	0.05114	1360	2.3819	0.05241
880	2.45342	0.05063	1370	2.38579	0.05377
890	2.44982	0.05033	1380	2.38994	0.0542
900	2.44652	0.05019	1390	2.39413	0.05367
910	2.44354	0.05016	1400	2.39813	0.05224
920	2.44086	0.05021	1410	2.40176	0.05
930	2.43848	0.0503	1420	2.40487	0.04709

1430	2.40736	0.04368	1780	2.36861	7.72568E-4
1440	2.40918	0.03992	1790	2.3679	7.43137E-4
1450	2.41031	0.03598	1800	2.36721	7.15492E-4
1460	2.41079	0.03201	1810	2.36654	6.89441E-4
1470	2.41067	0.02813	1820	2.36589	6.6483E-4
1480	2.41001	0.02445	1830	2.36526	6.4153E-4
1490	2.40891	0.02103	1840	2.36464	6.19433E-4
1500	2.40746	0.01792	1850	2.36404	5.98445E-4
1510	2.40574	0.01515	1860	2.36346	5.78485E-4
1520	2.40383	0.01273	1870	2.36288	5.59483E-4
1530	2.40181	0.01064	1880	2.36232	5.41373E-4
1540	2.39973	0.00886	1890	2.36178	5.24099E-4
1550	2.39765	0.00737	1900	2.36124	5.07608E-4
1560	2.3956	0.00614	1910	2.36072	4.91854E-4
1570	2.3936	0.00512	1920	2.36021	4.76791E-4
1580	2.39169	0.00429	1930	2.35971	4.62379E-4
1590	2.38986	0.00362	1940	2.35922	4.48582E-4
1600	2.38813	0.00309	1950	2.35874	4.35365E-4
1610	2.38649	0.00266	1960	2.35827	4.22695E-4
1620	2.38494	0.00231	1970	2.35781	4.10543E-4
1630	2.38348	0.00204	1980	2.35736	3.98881E-4
1640	2.38211	0.00182	1990	2.35691	3.87682E-4
1650	2.38081	0.00164	2000	2.35647	3.76924E-4
1660	2.37959	0.00149	2010	2.35605	3.66583E-4
1670	2.37843	0.00138	2020	2.35562	3.56637E-4
1680	2.37733	0.00128	2030	2.35521	3.47068E-4
1690	2.37628	0.00119	2040	2.3548	3.37856E-4
1700	2.37528	0.00112	2050	2.3544	3.28984E-4
1710	2.37433	0.00106	2060	2.35401	3.20435E-4
1720	2.37342	0.00101	2070	2.35363	3.12195E-4
1730	2.37254	9.57595E-4	2080	2.35324	3.04248E-4
1740	2.3717	9.14004E-4	2090	2.35287	2.96581E-4
1750	2.37089	8.74293E-4	2100	2.3525	2.89181E-4
1760	2.3701	8.378E-4			
1770	2.36935	8.04021E-4			

6.7. PbS 1370 – NH_4I capping

450	3.39198	0.60482	950	2.93106	0.0783
460	3.34321	0.57081	960	2.92734	0.07725
470	3.30243	0.54637	970	2.92398	0.0763
480	3.26951	0.5283	980	2.92098	0.07538
490	3.24375	0.51409	990	2.91831	0.07445
500	3.22413	0.50188	1000	2.91595	0.07345
510	3.20949	0.49039	1010	2.91386	0.07233
520	3.19876	0.47886	1020	2.912	0.07107
530	3.19094	0.46685	1030	2.91031	0.06965
540	3.18527	0.45424	1040	2.90875	0.06804
550	3.1812	0.44107	1050	2.90726	0.06625
560	3.17858	0.42747	1060	2.90581	0.06427
570	3.17777	0.41264	1070	2.90436	0.06213
580	3.17716	0.39583	1080	2.90285	0.05983
590	3.17589	0.37772	1090	2.90126	0.0574
600	3.17361	0.35883	1100	2.89957	0.05486
610	3.17014	0.33963	1110	2.89775	0.05224
620	3.16546	0.3205	1120	2.89578	0.04957
630	3.15959	0.30176	1130	2.89366	0.04687
640	3.15263	0.28366	1140	2.89137	0.04416
650	3.14471	0.26641	1150	2.88891	0.04147
660	3.13599	0.25018	1160	2.88627	0.03883
670	3.12665	0.23507	1170	2.88344	0.03625
680	3.11686	0.22115	1180	2.88043	0.03374
690	3.10683	0.20844	1190	2.87722	0.03133
700	3.09671	0.19692	1200	2.87379	0.02903
710	3.08668	0.18653	1210	2.8701	0.02686
720	3.07686	0.17719	1220	2.86612	0.02485
730	3.06738	0.16878	1230	2.86178	0.02307
740	3.05831	0.1612	1240	2.85702	0.02161
750	3.04969	0.1543	1250	2.85177	0.02066
760	3.04154	0.14797	1260	2.84605	0.02044
770	3.03385	0.14209	1270	2.83995	0.02126
780	3.02659	0.13655	1280	2.83371	0.02342
790	3.01971	0.13128	1290	2.82778	0.02719
800	3.01315	0.12622	1300	2.82274	0.03265
810	3.00683	0.12133	1310	2.81928	0.03963
820	3.0007	0.11659	1320	2.81803	0.04763
830	2.9947	0.11202	1330	2.81943	0.05589
840	2.98878	0.10763	1340	2.82357	0.06344
850	2.98293	0.10344	1350	2.83012	0.06934
860	2.97712	0.09951	1360	2.83839	0.07282
870	2.97136	0.09585	1370	2.84747	0.07347
880	2.96566	0.09251	1380	2.85635	0.07125
890	2.96007	0.08951	1390	2.86414	0.06652
900	2.95462	0.08686	1400	2.87021	0.05986
910	2.94936	0.08455	1410	2.87419	0.05203
920	2.94433	0.08258	1420	2.87603	0.04377
930	2.93958	0.08091	1430	2.87591	0.0357
940	2.93515	0.0795	1440	2.87417	0.02832

1450	2.87122	0.0219	1780	2.80395	3.62932E-4
1460	2.86748	0.01658	1790	2.80309	3.48416E-4
1470	2.86333	0.01234	1800	2.80226	3.34751E-4
1480	2.85906	0.00909	1810	2.80145	3.2187E-4
1490	2.85487	0.00667	1820	2.80065	3.09711E-4
1500	2.8509	0.00492	1830	2.79988	2.98219E-4
1510	2.84722	0.00369	1840	2.79913	2.87345E-4
1520	2.84385	0.00283	1850	2.79839	2.77042E-4
1530	2.84078	0.00224	1860	2.79768	2.6727E-4
1540	2.83798	0.00183	1870	2.79698	2.57991E-4
1550	2.83543	0.00155	1880	2.79629	2.49171E-4
1560	2.8331	0.00135	1890	2.79562	2.40779E-4
1570	2.83094	0.0012	1900	2.79497	2.32787E-4
1580	2.82894	0.00109	1910	2.79433	2.25168E-4
1590	2.82708	0.001	1920	2.7937	2.17899E-4
1600	2.82533	9.29897E-4	1930	2.79309	2.10958E-4
1610	2.82367	8.67181E-4	1940	2.79249	2.04325E-4
1620	2.8221	8.12213E-4	1950	2.7919	1.97981E-4
1630	2.82061	7.63173E-4	1960	2.79133	1.91909E-4
1640	2.81919	7.18887E-4	1970	2.79076	1.86094E-4
1650	2.81783	6.78565E-4	1980	2.79021	1.8052E-4
1660	2.81652	6.41646E-4	1990	2.78967	1.75176E-4
1670	2.81527	6.07707E-4	2000	2.78914	1.70047E-4
1680	2.81406	5.76414E-4	2010	2.78862	1.65123E-4
1690	2.81289	5.47491E-4	2020	2.78811	1.60393E-4
1700	2.81177	5.20702E-4	2030	2.78761	1.55846E-4
1710	2.81068	4.95842E-4	2040	2.78712	1.51474E-4
1720	2.80963	4.72731E-4	2050	2.78663	1.47267E-4
1730	2.80861	4.51209E-4	2060	2.78616	1.43217E-4
1740	2.80762	4.31134E-4	2070	2.7857	1.39318E-4
1750	2.80666	4.12377E-4	2080	2.78524	1.35561E-4
1760	2.80573	3.94825E-4	2090	2.78479	1.31939E-4
1770	2.80483	3.78374E-4	2100	2.78435	1.28448E-4

6.8. PbS 1370 – OA

450	2.16791	0.19783	950	2.05868	0.03865
460	2.1622	0.19265	960	2.0577	0.03819
470	2.15749	0.18766	970	2.0568	0.03771
480	2.15357	0.18275	980	2.05596	0.03722
490	2.15024	0.17785	990	2.05519	0.0367
500	2.14734	0.17296	1000	2.05446	0.03615
510	2.14475	0.1681	1010	2.05378	0.03558
520	2.14239	0.16333	1020	2.05313	0.03499
530	2.14023	0.15871	1030	2.05251	0.03437
540	2.13833	0.15432	1040	2.05191	0.03373
550	2.13688	0.1502	1050	2.05132	0.03306
560	2.13611	0.14583	1060	2.05074	0.03238
570	2.13549	0.14099	1070	2.05017	0.03167
580	2.1348	0.13583	1080	2.04959	0.03095
590	2.13394	0.13045	1090	2.04901	0.03022
600	2.13283	0.12494	1100	2.04842	0.02948
610	2.13145	0.1194	1110	2.04782	0.02873
620	2.12978	0.11389	1120	2.04721	0.02798
630	2.12781	0.10847	1130	2.04658	0.02722
640	2.12555	0.10323	1140	2.04594	0.02646
650	2.123	0.09824	1150	2.04527	0.02571
660	2.1202	0.09356	1160	2.04458	0.02495
670	2.11722	0.08927	1170	2.04386	0.02421
680	2.11414	0.08542	1180	2.04312	0.02347
690	2.11109	0.082	1190	2.04233	0.02273
700	2.10816	0.079	1200	2.04151	0.02201
710	2.10546	0.07632	1210	2.04064	0.0213
720	2.10302	0.07386	1220	2.03972	0.02061
730	2.10085	0.0715	1230	2.03871	0.01994
740	2.0989	0.06913	1240	2.03762	0.0193
750	2.09708	0.0667	1250	2.0364	0.01871
760	2.09529	0.06418	1260	2.03503	0.01822
770	2.09345	0.06159	1270	2.03349	0.01788
780	2.0915	0.05899	1280	2.03178	0.01779
790	2.08941	0.05645	1290	2.02993	0.01807
800	2.08717	0.05403	1300	2.02804	0.01883
810	2.08481	0.0518	1310	2.02629	0.02015
820	2.08239	0.04978	1320	2.0249	0.02206
830	2.07993	0.048	1330	2.02412	0.02446
840	2.0775	0.04646	1340	2.02417	0.02717
850	2.07514	0.04514	1350	2.02519	0.02986
860	2.07288	0.04403	1360	2.02716	0.03217
870	2.07075	0.0431	1370	2.02993	0.03378
880	2.06876	0.0423	1380	2.0332	0.03444
890	2.06691	0.04163	1390	2.03661	0.03402
900	2.06521	0.04103	1400	2.0398	0.03259
910	2.06366	0.04051	1410	2.04245	0.03031
920	2.06223	0.04002	1420	2.04436	0.02745
930	2.06094	0.03956	1430	2.04547	0.0243
940	2.05976	0.0391	1440	2.04579	0.02113

1450	2.04544	0.01815	1780	2.02008	0.00264
1460	2.04457	0.01551	1790	2.0197	0.00255
1470	2.04336	0.01327	1800	2.01934	0.00247
1480	2.04194	0.01144	1810	2.01898	0.00239
1490	2.04045	0.01	1820	2.01864	0.00231
1500	2.03897	0.00888	1830	2.01829	0.00224
1510	2.03755	0.00802	1840	2.01796	0.00217
1520	2.03624	0.00736	1850	2.01764	0.0021
1530	2.03503	0.00685	1860	2.01732	0.00203
1540	2.03392	0.00645	1870	2.017	0.00197
1550	2.03292	0.00612	1880	2.0167	0.00191
1560	2.032	0.00584	1890	2.0164	0.00185
1570	2.03115	0.00559	1900	2.0161	0.0018
1580	2.03036	0.00537	1910	2.01582	0.00174
1590	2.02962	0.00516	1920	2.01553	0.00169
1600	2.02892	0.00497	1930	2.01526	0.00164
1610	2.02827	0.00479	1940	2.01499	0.00159
1620	2.02764	0.00462	1950	2.01472	0.00155
1630	2.02704	0.00445	1960	2.01446	0.0015
1640	2.02647	0.00429	1970	2.0142	0.00146
1650	2.02591	0.00414	1980	2.01395	0.00142
1660	2.02538	0.00399	1990	2.01371	0.00138
1670	2.02487	0.00385	2000	2.01347	0.00134
1680	2.02437	0.00372	2010	2.01323	0.0013
1690	2.02388	0.00359	2020	2.01299	0.00127
1700	2.02341	0.00347	2030	2.01277	0.00123
1710	2.02296	0.00335	2040	2.01254	0.0012
1720	2.02251	0.00323	2050	2.01232	0.00116
1730	2.02208	0.00312	2060	2.0121	0.00113
1740	2.02166	0.00302	2070	2.01189	0.0011
1750	2.02125	0.00292	2080	2.01168	0.00108
1760	2.02085	0.00282	2090	2.01148	0.00105
1770	2.02046	0.00273	2100	2.01127	0.00102

6.9. PbS 1450 – OA capping

450	2.33297	0.34978	950	2.18794	0.06435
460	2.3359	0.33267	960	2.18659	0.06411
470	2.33752	0.31534	970	2.18541	0.06392
480	2.33773	0.29812	980	2.18439	0.06374
490	2.33652	0.28132	990	2.18351	0.06356
500	2.33397	0.26527	1000	2.18278	0.06337
510	2.33023	0.25025	1010	2.18218	0.06315
520	2.32556	0.23653	1020	2.18169	0.06289
530	2.32033	0.22437	1030	2.18131	0.06258
540	2.31532	0.2139	1040	2.18102	0.06221
550	2.31116	0.20393	1050	2.18081	0.06178
560	2.30696	0.19408	1060	2.18066	0.06129
570	2.30248	0.18457	1070	2.18057	0.06072
580	2.29768	0.17558	1080	2.18051	0.06009
590	2.2926	0.16722	1090	2.18048	0.05939
600	2.28732	0.15957	1100	2.18047	0.05862
610	2.28197	0.15268	1110	2.18046	0.05778
620	2.27666	0.14653	1120	2.18045	0.05689
630	2.2715	0.14108	1130	2.18043	0.05594
640	2.26658	0.13628	1140	2.1804	0.05493
650	2.26199	0.13203	1150	2.18034	0.05388
660	2.25777	0.12824	1160	2.18025	0.05279
670	2.25393	0.12479	1170	2.18012	0.05166
680	2.25049	0.12159	1180	2.17996	0.0505
690	2.24741	0.11855	1190	2.17975	0.04931
700	2.24465	0.11559	1200	2.17949	0.0481
710	2.24215	0.11265	1210	2.17918	0.04687
720	2.23986	0.10968	1220	2.17882	0.04563
730	2.23771	0.10668	1230	2.1784	0.04439
740	2.23564	0.10363	1240	2.17792	0.04314
750	2.23359	0.10053	1250	2.17737	0.04189
760	2.23153	0.09741	1260	2.17675	0.04066
770	2.22941	0.0943	1270	2.17605	0.03943
780	2.22721	0.09123	1280	2.17527	0.03823
790	2.22492	0.08823	1290	2.17439	0.03706
800	2.22254	0.08534	1300	2.1734	0.03595
810	2.22006	0.08259	1310	2.1723	0.03491
820	2.21751	0.08001	1320	2.17108	0.03397
830	2.2149	0.07761	1330	2.16974	0.03316
840	2.21226	0.07543	1340	2.16829	0.03254
850	2.20961	0.07346	1350	2.16676	0.03215
860	2.20698	0.07171	1360	2.16519	0.03203
870	2.20439	0.07019	1370	2.16364	0.03221
880	2.20188	0.06888	1380	2.16218	0.03271
890	2.19947	0.06777	1390	2.16091	0.03355
900	2.19717	0.06685	1400	2.15991	0.03468
910	2.19501	0.0661	1410	2.15927	0.03604
920	2.193	0.06549	1420	2.15907	0.03755
930	2.19114	0.06502	1430	2.15935	0.03911
940	2.18946	0.06464	1440	2.16012	0.04058

1450	2.16135	0.04184	1780	2.15809	0.0055
1460	2.163	0.04278	1790	2.15738	0.00528
1470	2.16496	0.0433	1800	2.1567	0.00507
1480	2.16712	0.04335	1810	2.15604	0.00487
1490	2.16936	0.04288	1820	2.1554	0.00468
1500	2.17156	0.04191	1830	2.15479	0.0045
1510	2.1736	0.04048	1840	2.1542	0.00433
1520	2.17539	0.03864	1850	2.15363	0.00416
1530	2.17686	0.03649	1860	2.15307	0.00401
1540	2.17796	0.0341	1870	2.15253	0.00386
1550	2.17867	0.03158	1880	2.15201	0.00372
1560	2.17899	0.02902	1890	2.1515	0.00358
1570	2.17896	0.02648	1900	2.15101	0.00345
1580	2.17861	0.02404	1910	2.15053	0.00332
1590	2.17798	0.02175	1920	2.15006	0.0032
1600	2.17713	0.01963	1930	2.14961	0.00309
1610	2.17611	0.0177	1940	2.14916	0.00298
1620	2.17496	0.01598	1950	2.14873	0.00287
1630	2.17373	0.01446	1960	2.14831	0.00277
1640	2.17246	0.01313	1970	2.1479	0.00267
1650	2.17118	0.01198	1980	2.1475	0.00258
1660	2.1699	0.01099	1990	2.1471	0.00249
1670	2.16866	0.01013	2000	2.14672	0.0024
1680	2.16745	0.00939	2010	2.14635	0.00232
1690	2.1663	0.00875	2020	2.14598	0.00224
1700	2.16519	0.0082	2030	2.14562	0.00216
1710	2.16414	0.00772	2040	2.14528	0.00209
1720	2.16314	0.0073	2050	2.14494	0.00202
1730	2.16219	0.00692	2060	2.1446	0.00195
1740	2.16129	0.00658	2070	2.14428	0.00189
1750	2.16043	0.00628	2080	2.14396	0.00182
1760	2.15962	0.006	2090	2.14365	0.00176
1770	2.15884	0.00574	2100	2.14335	0.0017

6.10. PbS 1550 – EDT

450	2.72212	0.70877
460	2.7145	0.68459
470	2.70843	0.66268
480	2.70385	0.64226
490	2.70051	0.62274
500	2.69806	0.60369
510	2.69612	0.58487
520	2.69433	0.56619
530	2.6924	0.54767
540	2.69011	0.52941
550	2.68732	0.51158
560	2.68397	0.49431
570	2.68007	0.47778
580	2.67568	0.46211
590	2.67089	0.44742
600	2.66583	0.43379
610	2.66065	0.42127
620	2.65551	0.4099
630	2.65058	0.39968
640	2.64611	0.3906
650	2.64238	0.38264
660	2.64004	0.37566
670	2.63938	0.36826
680	2.63934	0.36007
690	2.63951	0.35123
700	2.63965	0.34187
710	2.63962	0.33208
720	2.6393	0.32197
730	2.6386	0.31163
740	2.63747	0.30115
750	2.63586	0.29061
760	2.63374	0.28011
770	2.63112	0.26973
780	2.62798	0.25954
790	2.62433	0.24963
800	2.62021	0.24005
810	2.61564	0.23087
820	2.61065	0.22216
830	2.60531	0.21395
840	2.59965	0.2063
850	2.59375	0.19924
860	2.58766	0.1928
870	2.58144	0.18698
880	2.57518	0.1818
890	2.56893	0.17726
900	2.56276	0.17333
910	2.55674	0.17001
920	2.55091	0.16725
930	2.54535	0.16502
940	2.54009	0.16328
950	2.53516	0.16198
960	2.53062	0.16107
970	2.52648	0.16049
980	2.52275	0.16018
990	2.51945	0.1601
1000	2.51658	0.16017
1010	2.51413	0.16035
1020	2.51209	0.16059
1030	2.51044	0.16085
1040	2.50917	0.16107
1050	2.50824	0.16122
1060	2.50762	0.16126
1070	2.50729	0.16118
1080	2.50721	0.16094
1090	2.50735	0.16052
1100	2.50767	0.15992
1110	2.50813	0.15913
1120	2.50871	0.15813
1130	2.50938	0.15692
1140	2.51009	0.15552
1150	2.51083	0.15392
1160	2.51157	0.15212
1170	2.51228	0.15015
1180	2.51294	0.148
1190	2.51352	0.14569
1200	2.51402	0.14324
1210	2.51441	0.14065
1220	2.51466	0.13795
1230	2.51478	0.13514
1240	2.51474	0.13225
1250	2.51453	0.12928
1260	2.51413	0.12627
1270	2.51353	0.12323
1280	2.51272	0.12018
1290	2.51168	0.11716
1300	2.5104	0.11419
1310	2.50888	0.1113
1320	2.50711	0.10854
1330	2.50509	0.10596
1340	2.50283	0.1036
1350	2.50035	0.1015
1360	2.49768	0.09973
1370	2.49486	0.09834
1380	2.49194	0.09736
1390	2.489	0.09684
1400	2.48611	0.0968
1410	2.48336	0.09725
1420	2.48083	0.09818
1430	2.47863	0.09957

1440	2.47684	0.10136
1450	2.47554	0.10349
1460	2.47481	0.10588
1470	2.47469	0.10841
1480	2.47521	0.11099
1490	2.47638	0.1135
1500	2.47817	0.11582
1510	2.48056	0.11784
1520	2.48348	0.11946
1530	2.48686	0.1206
1540	2.49059	0.12118
1550	2.49458	0.12117
1560	2.49872	0.12054
1570	2.5029	0.11927
1580	2.50703	0.11739
1590	2.51101	0.11492
1600	2.51475	0.11191
1610	2.51818	0.10842
1620	2.52124	0.1045
1630	2.5239	0.10024
1640	2.5261	0.0957
1650	2.52785	0.09095
1660	2.52914	0.08608
1670	2.52996	0.08114
1680	2.53034	0.0762
1690	2.53029	0.07132
1700	2.52985	0.06653
1710	2.52905	0.06189
1720	2.52793	0.05742
1730	2.52651	0.05316
1740	2.52485	0.04911
1750	2.52298	0.04531
1760	2.52093	0.04174
1770	2.51874	0.03842
1780	2.51644	0.03534
1790	2.51407	0.0325
1800	2.51164	0.02989
1810	2.50917	0.02749
1820	2.5067	0.02531
1830	2.50424	0.02332
1840	2.5018	0.02152
1850	2.49939	0.01988
1860	2.49702	0.0184
1870	2.49471	0.01706
1880	2.49245	0.01585
1890	2.49025	0.01475
1900	2.48811	0.01376
1910	2.48604	0.01286
1920	2.48403	0.01205
1930	2.48209	0.01131
1940	2.48022	0.01064
1950	2.4784	0.01003
1960	2.47665	0.00947
1970	2.47495	0.00896
1980	2.47332	0.0085
1990	2.47173	0.00807
2000	2.4702	0.00767
2010	2.46872	0.0073
2020	2.46729	0.00696
2030	2.4659	0.00665
2040	2.46455	0.00635
2050	2.46325	0.00608
2060	2.46198	0.00582
2070	2.46075	0.00557
2080	2.45956	0.00534
2090	2.4584	0.00513
2100	2.45727	0.00492

6.11. PbS 1550 – NH_4I capping

450	2.87743	0.85015	950	2.83374	0.1689
460	2.88942	0.83366	960	2.82973	0.16661
470	2.90135	0.81326	970	2.82598	0.16457
480	2.91164	0.79041	980	2.8225	0.16276
490	2.91967	0.76666	990	2.81931	0.16113
500	2.92555	0.74332	1000	2.81641	0.15966
510	2.92986	0.72127	1010	2.81379	0.15831
520	2.93338	0.7009	1020	2.81146	0.15704
530	2.93687	0.68217	1030	2.80941	0.15582
540	2.94091	0.66472	1040	2.80762	0.15462
550	2.94582	0.648	1050	2.80607	0.15342
560	2.95163	0.63142	1060	2.80476	0.15218
570	2.95815	0.61449	1070	2.80365	0.15089
580	2.96503	0.59685	1080	2.80274	0.14953
590	2.97184	0.57833	1090	2.80198	0.14807
600	2.97816	0.55893	1100	2.80137	0.14652
610	2.98366	0.53879	1110	2.80087	0.14485
620	2.98818	0.51813	1120	2.80046	0.14307
630	2.99151	0.49693	1130	2.80012	0.14117
640	2.99333	0.47554	1140	2.79983	0.13914
650	2.9936	0.45434	1150	2.79956	0.137
660	2.99238	0.43363	1160	2.79929	0.13474
670	2.98981	0.41369	1170	2.79901	0.13236
680	2.98608	0.3947	1180	2.7987	0.12989
690	2.9814	0.37679	1190	2.79833	0.12731
700	2.97597	0.36003	1200	2.7979	0.12465
710	2.97001	0.34442	1210	2.79739	0.12191
720	2.96368	0.32994	1220	2.79678	0.1191
730	2.95715	0.31653	1230	2.79607	0.11623
740	2.95053	0.30411	1240	2.79524	0.11332
750	2.94392	0.2926	1250	2.79429	0.11036
760	2.93738	0.28189	1260	2.79319	0.10739
770	2.93095	0.2719	1270	2.79194	0.1044
780	2.92465	0.26254	1280	2.79052	0.10141
790	2.91849	0.25375	1290	2.78892	0.09844
800	2.91246	0.24547	1300	2.78712	0.09551
810	2.90655	0.23764	1310	2.78511	0.09265
820	2.90074	0.23025	1320	2.78286	0.08988
830	2.89502	0.22325	1330	2.78036	0.08725
840	2.88938	0.21665	1340	2.7776	0.0848
850	2.8838	0.21043	1350	2.77458	0.08259
860	2.87829	0.2046	1360	2.77131	0.0807
870	2.87286	0.19914	1370	2.76781	0.07919
880	2.86749	0.19407	1380	2.76413	0.07814
890	2.86223	0.18938	1390	2.76034	0.07763
900	2.85707	0.18507	1400	2.75653	0.07772
910	2.85204	0.18114	1410	2.75282	0.07846
920	2.84717	0.17757	1420	2.74934	0.07986
930	2.84249	0.17435	1430	2.74624	0.08191
940	2.838	0.17147	1440	2.74367	0.08456

1450	2.74178	0.08772	1780	2.76915	0.01845
1460	2.74069	0.09125	1790	2.76638	0.01682
1470	2.7405	0.09501	1800	2.7637	0.0154
1480	2.74124	0.09879	1810	2.7611	0.01414
1490	2.74294	0.10241	1820	2.7586	0.01305
1500	2.74556	0.10566	1830	2.75619	0.01208
1510	2.749	0.10837	1840	2.75388	0.01122
1520	2.75314	0.11036	1850	2.75167	0.01047
1530	2.75782	0.11153	1860	2.74955	0.0098
1540	2.76286	0.11178	1870	2.74752	0.0092
1550	2.76806	0.11108	1880	2.74558	0.00866
1560	2.77325	0.10944	1890	2.74371	0.00817
1570	2.77824	0.10689	1900	2.74192	0.00773
1580	2.78288	0.10351	1910	2.7402	0.00733
1590	2.78704	0.09941	1920	2.73855	0.00696
1600	2.79061	0.09472	1930	2.73696	0.00662
1610	2.79354	0.08956	1940	2.73543	0.0063
1620	2.79576	0.08407	1950	2.73395	0.00601
1630	2.79729	0.07839	1960	2.73252	0.00573
1640	2.79812	0.07263	1970	2.73114	0.00548
1650	2.7983	0.06691	1980	2.7298	0.00523
1660	2.79788	0.06132	1990	2.7285	0.005
1670	2.7969	0.05595	2000	2.72725	0.00479
1680	2.79546	0.05084	2010	2.72603	0.00458
1690	2.79361	0.04606	2020	2.72484	0.00439
1700	2.79142	0.04162	2030	2.72369	0.0042
1710	2.78898	0.03754	2040	2.72257	0.00403
1720	2.78634	0.03383	2050	2.72147	0.00386
1730	2.78356	0.03047	2060	2.72041	0.0037
1740	2.78069	0.02747	2070	2.71937	0.00355
1750	2.77779	0.02478	2080	2.71836	0.0034
1760	2.77487	0.0224	2090	2.71737	0.00326
1770	2.77199	0.0203	2100	2.71641	0.00313

6.12. PbS 1550 – OA capping

450	2.22462	0.21365	950	2.05488	0.05507
460	2.20823	0.19597	960	2.05361	0.05464
470	2.19215	0.18181	970	2.05244	0.05429
480	2.17672	0.17081	980	2.05138	0.054
490	2.1622	0.16266	990	2.05042	0.05376
500	2.14885	0.15715	1000	2.04957	0.05355
510	2.13704	0.15413	1010	2.04883	0.05337
520	2.12741	0.1535	1020	2.04818	0.0532
530	2.12156	0.15405	1030	2.04763	0.05303
540	2.11813	0.15331	1040	2.04717	0.05285
550	2.11571	0.15151	1050	2.04679	0.05265
560	2.11379	0.14896	1060	2.04648	0.05244
570	2.11206	0.14591	1070	2.04624	0.05219
580	2.11041	0.14255	1080	2.04607	0.05191
590	2.10875	0.13904	1090	2.04594	0.0516
600	2.10708	0.13549	1100	2.04586	0.05124
610	2.1054	0.13198	1110	2.04581	0.05084
620	2.10373	0.12856	1120	2.04579	0.05039
630	2.10211	0.12523	1130	2.04579	0.0499
640	2.10054	0.12201	1140	2.04581	0.04937
650	2.09905	0.1189	1150	2.04583	0.04879
660	2.09764	0.11586	1160	2.04586	0.04817
670	2.09631	0.1129	1170	2.04588	0.04751
680	2.09506	0.10998	1180	2.04589	0.04681
690	2.09387	0.1071	1190	2.04588	0.04608
700	2.09273	0.10423	1200	2.04586	0.04532
710	2.09162	0.10138	1210	2.04581	0.04452
720	2.09053	0.09853	1220	2.04573	0.0437
730	2.08942	0.09569	1230	2.04561	0.04285
740	2.08828	0.09286	1240	2.04546	0.04199
750	2.08711	0.09005	1250	2.04527	0.0411
760	2.08587	0.08727	1260	2.04504	0.0402
770	2.08457	0.08453	1270	2.04475	0.0393
780	2.0832	0.08185	1280	2.04441	0.03839
790	2.08174	0.07924	1290	2.04401	0.03747
800	2.08022	0.07671	1300	2.04354	0.03657
810	2.07861	0.07429	1310	2.043	0.03568
820	2.07695	0.07199	1320	2.04238	0.03481
830	2.07522	0.06981	1330	2.04167	0.03398
840	2.07344	0.06778	1340	2.04088	0.03321
850	2.07164	0.06589	1350	2.03999	0.03252
860	2.06981	0.06415	1360	2.03901	0.03192
870	2.06798	0.06257	1370	2.03795	0.03145
880	2.06616	0.06114	1380	2.03682	0.03114
890	2.06436	0.05987	1390	2.03565	0.031
900	2.06261	0.05875	1400	2.03446	0.03107
910	2.06091	0.05776	1410	2.0333	0.03136
920	2.05928	0.05691	1420	2.03222	0.03188
930	2.05772	0.05619	1430	2.03126	0.03262
940	2.05625	0.05558	1440	2.03048	0.03357

1450	2.02993	0.03471
1460	2.02965	0.03598
1470	2.02968	0.03734
1480	2.03005	0.03872
1490	2.03075	0.04004
1500	2.03177	0.04125
1510	2.0331	0.04227
1520	2.03468	0.04304
1530	2.03646	0.04353
1540	2.03839	0.04369
1550	2.0404	0.04351
1560	2.0424	0.04298
1570	2.04435	0.04212
1580	2.04619	0.04095
1590	2.04786	0.03951
1600	2.04932	0.03784
1610	2.05055	0.03599
1620	2.05153	0.034
1630	2.05225	0.03193
1640	2.05271	0.02982
1650	2.05293	0.02772
1660	2.05293	0.02565
1670	2.05272	0.02365
1680	2.05232	0.02174
1690	2.05178	0.01994
1700	2.0511	0.01827
1710	2.05032	0.01673
1720	2.04946	0.01531
1730	2.04854	0.01403
1740	2.04759	0.01287
1750	2.04661	0.01183
1760	2.04563	0.01091
1770	2.04465	0.01008
1780	2.04369	0.00935
1790	2.04274	0.00869
1800	2.04182	0.00812
1810	2.04093	0.0076
1820	2.04008	0.00715
1830	2.03925	0.00674
1840	2.03846	0.00638
1850	2.0377	0.00605
1860	2.03697	0.00575
1870	2.03627	0.00548
1880	2.0356	0.00524
1890	2.03496	0.00501
1900	2.03434	0.0048
1910	2.03375	0.00461
1920	2.03318	0.00443
1930	2.03263	0.00426
1940	2.0321	0.0041
1950	2.03159	0.00395
1960	2.03109	0.0038
1970	2.03061	0.00367
1980	2.03014	0.00354
1990	2.02969	0.00342
2000	2.02926	0.0033
2010	2.02883	0.00319
2020	2.02841	0.00308
2030	2.02801	0.00297
2040	2.02762	0.00287
2050	2.02723	0.00278
2060	2.02686	0.00269
2070	2.02649	0.0026
2080	2.02614	0.00251
2090	2.02579	0.00243
2100	2.02545	0.00235